TÉCNICO LISBOA

100 Gb/s SSB MB-OFDM metropolitan networks employing memory polynomials for SSBI mitigation

Gonçalo Azevedo Martinho

Thesis to obtain the Master of Science Degree in

Electrical and Computer Engineering

Supervisors: Prof. Dr. Adolfo da Visitação Tregeira Cartaxo
Dr. Tiago Manuel Ferreira Alves

Examination Committee

Chairperson: Prof. Dr. José Eduardo Charters Ribeiro da Cunha Sanguino
Supervisor: Dr. Tiago Manuel Ferreira Alves
Members of the Committee: Prof. Dr. Paulo Miguel Nepomuceno Pereira Monteiro

May 2016

This dissertation was performed under the project “Metro networks based on multi-band orthogonal frequency-division multiplexing signals” (MORFEUS-PTDC/EEI-TEL/2573/2012) funded by Fundação para a Ciência e Tecnologia from Portugal, under the supervision of

Prof. Dr. Adolfo da Visitação Tregeira Cartaxo
Dr. Tiago Manuel Ferreira Alves

Acknowledgements

Firstly, I would like to thank my family, especially my parents Rogério and Cristina for their unconditional support through my work on this dissertation. Without their support and unlimited patience, the conclusion of this dissertation would not have been possible.

Secondly, I would like to thank my supervisor, Associate Professor Adolfo Cartaxo and co-supervisor Ph. D. Tiago Alves for their support and guidance provided during the execution of this dissertation.

Thirdly, I would like to thank Ph. D. Student Pedro Cruz for his support with knowledge and access to the simulation PCs that allowed me to achieve the 100% complete simulations.

Lastly, I would like to thank my friends, Marcos Caldeira e Cátia Pereira, for all their support.

Abstract

In this dissertation, it is assessed the performance of a system employing a 100 Gbit/s single sideband (SSB) multi-band orthogonal frequency division multiplexing (MB-OFDM) signal. This SSB signal, used to neglect the effect of the chromatic dispersion induced power fading (CDIPF) is created on the dual-parallel Mach Zehnder modulator (DP-MZM). The system uses direct-detection (DD) at the receiver, in which the distortion signal-signal beat interference (SSBI) is originated. With the use of memory polynomials (MP), it is evaluated if this performance issue can be mitigated, determining the required optical-signal-noise ratio (OSNR) that achieves a bit error rate of 10^{-3}.

Two MB-OFDM systems were considered. The first one was designed to singly evaluate the performance improvement achieved by the MP. In this noise free single-band system, it was achieved an improvement of approximately ~7 dB on the system EVM. On the second system, both electrical and optical noise, SB and MB were considered, as well as the use of a nonlinear band selector and optical fibre. The configurations tested varied from ideal band selector and B2B configuration to a more realist system employing a nonlinear band selector, 2^{nd} order super Gaussian model, and optical fibre, standard single-mode fibre (SSMF) model. This was meant to determine the minimum required OSNR to achieve a BER of 10^{-3}. Despite the improvement of EVM achieved on the first test, the second showed a decrease in system EVM, caused primarily by the system MB configuration. It showed also the impossibility to achieve the BER of 10^{-3}.

Keywords: multi band (MB), orthogonal frequency division multiplexing (OFDM), dual-parallel Mach-Zehnder modulator (DP-MZM), single side band (SSB), direct detection (DD), positive intrinsic negative (PIN), signal-signal beat interference (SSBI), memory polynomials (MP).

Resumo

Esta dissertação tem como objetivo estudar um sistema ótico constituído por um sinal multi-banda (MB) com multiplexagem ortogonal por divisão ortogonal na frequência (OFDM). Este sinal, constituído por um ritmo binário de 100 Gbit/s e por uma configuração de banda unilateral (SSB) usada para corrigir a distorção causada pela dispersão cromática, é criado no modulador ótico paralelo duplo de Mach Zehnder (DP-MZM). Este sistema usa na receção um sistema de deteção direta, onde a conversão ótica para elétrica é feita através de um conversor positivo-intrínseco-negativo (PIN). Ao utilizar este conversor é adicionado ao sinal convertido uma distorção chamada batimento sinal-sinal (SSBI), degradando o sinal que será posteriormente processado no recetor. Para corrigir este efeito é proposto avaliar a possibilidade de correção através de polinómios com memória, determinando qual a relação sinal-ruído ótica (OSNR) capaz de atingir um erro de bit (BER) de 10^{-3}.

Para avaliar a capacidade de mitigação do SSBI com MPs, foram conduzidos 2 testes separados. No primeiro foi apenas avaliada a capacidade de mitigação de SSBI sem considerar qualquer tipo de ruído e considerando apenas uma banda OFDM. Neste caso houve uma redução em 7 dB na degradação do sinal causado pelo SSBI. Porém, no segundo teste foram consideradas quatro configurações de sistema. Estas quatro configurações variaram entre seletor de banda ideal ou não ideal e com e sem fibra ótica. Em qualquer caso considerado, o sistema desenvolvido não foi capaz de mitigar corretamente o SSBI e assim não atingiu o erro de bit mínimo de 10^{-3}.

Palavras-chave: multi-banda (MB), multiplexagem ortogonal por divisão na frequência (OFDM), modulador duplo paralelo de Mach Zehnder (DP-MZM), banda lateral simples (SSB), deteção direta (DD), positivo-intrínseco-negativo (PIN), batimento sinal-sinal (SSBI), polinómios com memória (MP).

Table of contents

List of tables

List of figures

List of Acronyms

Acronym	Description
ADC	Analog-to-Digital Converter
ASE	Amplified spontaneous emission
B2B	Back-to-back
BER	Bit Error Ratio
BG	Band gap
BS	Band selector
CD	Chromatic Dispersion
CDIPF	Chromatic Dispersion Induced Power Fading
CO-OFDM	Coherent Optical Orthogonal Frequency Division Multiplexing
CP	Cyclic Prefix
DAC	Digital-to-Analog Converter
DC	Direct Current
DD	Direct Detection
DDO-OFDM	Direct Detection Optical Orthogonal Frequency Division Multiplexing
DFT	Discrete Fourier Transform
DPD	Digital Pre-distortion
DP-MZM	Dual-parallel Mach Zehnder Modulator
DPostD	Digital Post-distortion
DSP	Digital Signal Processor
DVB	Digital Video Broadcasting
DVK	Discrete Volterra Kernel
EDFA	Erbium Doped Fibre Amplifier
EGA	Exhaustive Gaussian approach
EVM	Error Vector Magnitude
FEC	Forward Error Correction
FFT	Fast Fourier Transform
FWM	Four Wave Mixing
GMP	Generalized Memory Polynomials
GVD	Group Velocity Dispersion
I/Q	In-phase/Quadrature
ICI	Inter-Carrier Interference
IDFT	Inverse-Discrete Fourier Transform
IFFT	Inverse-Fast Fourier Transform
ISI	Inter-Symbol Interference
LR-PON	Long-reach passive optical network
MB	Multi-Band
MBP	Minimum bias point
MB-OFDM	Multi-Band Orthogonal Frequency Division Multiplexing
MCM	Multicarrier Modulation
MEB	MORFEUS Extraction Block
MIB	MORFEUS Insertion Block

MORFEUS	Metro Networks Based on Multi-Band Orthogonal Frequency Division Multiplexing Signals
MP	Memory Polynomials
MZM	Mach Zehnder Modulator
NLD	Non Linear Dispersion
OF	Optical Filter
OFDM	Orthogonal Frequency Division Multiplexing
OSNR	Optical Signal-to-Noise Ratio
PAPR	Peak-to-Average Power Ratio
PIN	Positive-Intrinsic-Negative
PMD	Polarization mode dispersion
QAM	Quadrature Amplitude Modulation
QBP	Quadrature bias point
RF	Radio Frequency
RFT-OFDM	Radio Frequency Tone-Assisted Orthogonal Frequency Division Multiplexing
ROADM	Reconfigurable Optical Add and Drop Multiplexer
SB	Single Band
SCM	Single carrier modulation
S&H	Sample and hold
SNR	Signal-to-noise ratio
SPM	Self-Phase Modulation
SSB	Single Sideband
SSBI	Signal-to-Signal Beat Interference
SSMF	Standard Single Mode Fibre
VBG	Virtual Band Gap
VBPR	Virtual Carrier to Band Power Ratio
VC	Virtual Carrier
VSSB-OFDM	Virtual Single Sideband Orthogonal Frequency Division Multiplexing
WDM	Wavelength-Division Multiplexing
XPM	Cross Phase Modulation

Chapter 1 - Introduction

In this chapter, it is given an introduction on the topics that are studied in this dissertation. In section 1.1, it is presented the scope of work of the following dissertation. In section 1.2, the motivation for the work developed is addressed and the respective objectives are enumerated. In section 1.3, it is presented the structure of this report and in section 1.4 the main contributions of the work developed are covered.

1.1 Scope of work

Recently, multiband-orthogonal frequency division multiplexing (MB-OFDM) signals have been proposed to integrate the telecommunications systems. This happens because of their great benefits, like for example, the increase on bandwidth allocation and flexibility, high spectral efficiency, high granularity and high tolerance to linear fibre distortion effects. To keep the cost of the system low, direct-detection is used. This detection technique introduces a performance limitation on the system, the signal-to-signal beat interference. The focus of this work is to implement digital signal processing (DSP) algorithms, based on memory polynomials (MP), to mitigate the SSBI distortion.

1.1.1 Metro networks

The data traffic transferred over the telecommunication networks has increased during the last few years. The telecommunication networks are composed by the long-haul core, metropolitan (metro) and access networks. The metro (metropolitan) network is the interface between the core and the access networks. Therefore, it is responsible for transporting data between access networks and, when needed, transporting data to the core network. Since metro networks are responsible for processing all the traffic between the core and the access networks, it needs to be prepared to be highly flexible and scalable; it also needs to be able to reconfigure dynamically and, since the cost envisioned to these networks is reduced, the power consumption and the space occupied by the network elements also represent a constraint.

To reduce the cost and to increase power efficiency of the next generation access networks, network operators presented a solution of integrating the metro and access networks in a single hybrid

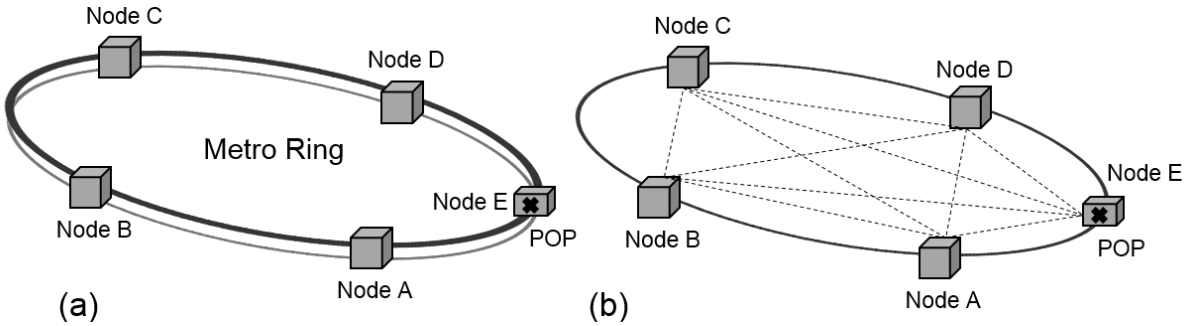

Figure 1.1 - (a) Physical topology of a metro network. (b) Logical topology of a metro network.

optical network [1-2], commonly known as long-reach passive optical network (LR-PON). This solution should be able to reduce the number of central offices and to increase the data rate delivered to the end users (a guaranteed data rate of 1 Gbit/s and a peak data rate of 10 Gbit/s [2]). Dynamic bandwidth allocation with various levels of granularity to meet the user's requirements is also envisioned to optimize the system capacity. The LR-PON is composed by two sub-networks: the feeder network, which can be viewed as the previous part of the network responsible for the traffic aggregation (metro) and the distribution network, responsible for transferring traffic to the end users.

Typically, the metro network architecture is based on the ring topology, represented in figure 1.1. Compared to other topologies [3-4], the ring is considered to be the most reliable. The example of figure 1.1 has five nodes and these nodes can be classified as edge, metro or pass-through nodes [5]. The edge nodes are responsible for adding or dropping traffic from the metro network to the access network. If there is no connection to the access network, the nodes are called metro nodes and, if the traffic is not affected by any node function, then the node is called a pass-through node. In figure 1.1 there is also represented a POP (point of presence) node. This node is used as interface to internet service providers. Besides being connected physically, the nodes of a metro network can also be connected logically, as represented in figure 1.1. The logical topology presented in the figure 1.1 (b) is the mesh topology.

Along the years, the wavelength division multiplexing (WDM) technique has provided accommodation for the increasing traffic demand. However, it does not support higher levels of granularity than the provided by a single optical channel. Therefore, there is the need for new techniques that would enable the routing with granularity at the sub-wavelength level in future transparent metro networks.

1.1.2 Introduction to OFDM

Orthogonal frequency division multiplexing (OFDM) has been recently referred as an advantageous modulation format to provide high-speed optical transmission and capacity granularity. This happens because of its high spectral efficiency and its resilience in the presence of fibre dispersion and PMD [6-7]. Therefore, it represents a great solution to mitigate inter-symbol interference (ISI), which is caused by a dispersive channel [8]. This is very important because, since data rates are increasing, serial modulation schemes like quadrature amplitude modulation (QAM) are used, and so, the received signal depends on multiple transmitted symbols [9]. Another advantage of OFDM is that it transfers the complexity of the transmitters and receivers from the analogue to the digital domain.

Although the OFDM systems are complex, as it will be shown in this report, the basic concept is simple [10-11]. Data is transmitted in parallel on a different number of frequencies, which are chosen to be mathematically orthogonal over one OFDM symbol period. As a result, the OFDM symbol period is longer than the one in the serial system, maintaining the same total data rate. Since the symbol period is longer, ISI affects less symbols, which simplifies equalization. To remove the residual ISI, most OFDM systems use a form of guard interval called cyclic prefix. Thanks to the almost rectangular shape of the

OFDM optical spectrum, multiple OFDM signals can be transmitted without guard band between them [12].

1.1.3 Types of OFDM detection

The two types of optical OFDM detection that have been considered are the direct detection optical OFDM (DDO-OFDM) and the coherent optical OFDM (CO-OFDM) [13].

In DDO-OFDM, the optical carrier is sent along with the OFDM signal. With this, it is only needed a photodiode to perform the conversion from optical to electrical. Because in this work, DDO-OFDM uses a photodiode, more specifically a positive-intrinsic-negative (PIN), which is presented in section 2.2.4, a signal distortion appears. This distortion is called SSBI, which is presented in section 2.2.4.

In CO-OFDM, there is no need to send the optical carrier with the signal. The optical carrier is suppressed, because the CO-OFDM receiver includes a local oscillator. However, with this, the frequency offset and phase noise sensitivity problem rises [14], which requires an extra phase and frequency offset estimation at the receiver. Although CO-OFDM has superior performance, with respect to signal-to-noise ratio (OSNR) requirements, and provides better spectral efficiency, it also requires an increase in receiver complexity.

Therefore, since the DDO-OFDM is less complex and less expensive to implement, it is the one preferred for metro networks.

1.1.4 Multiband-OFDM concept

Over the past years, the traffic in metro and core networks had an increase of 45% per year on average [15], due to the increase of multimedia and peer to peer applications. In order to withstand this increase, optical networks have evolved into WDM networks and link capacity of metro and core networks has been raised several terabit/s per fibre pair. Therefore, to gain from the network transparency and also to reduce the overall costs and consumption of the network [16], reconfigurable optical add and drop multiplexers (ROADM) have been deployed. Additionally, these all-optical transmission techniques allow for transparent managing and switching of full WDM channels without requiring the use of optical to electrical and electrical to optical converters (O-E-O). In transparent switching, the channels with traffic in transit cannot be shared with the add and drop traffic channels. The transparent switching allows the ROADMs to fully operate in optical mode. On the other hand, opaque switching offers total flexibility in the aggregation/disaggregation of traffic. However, since all of the channels need to be converted from optical to electrical and then back to optical, this leads to higher costs when compared to transparent nodes.

In this context, MB-OFDM with its confined and narrow spectrum represents the ideal candidate for future metro networks. This modulation technique offers a trade-off between capacity increase and electrical consumption. MB-OFDM can handle the 100 Gbit/s bitrates of the next generation optical networks, allowing to optically switch at the band granularity.

Despite the fact that optical OFDM systems have been widely studied, the implementation of MB-OFDM systems using DDO-OFDM is still a concept [17]. Although the system proposed in [17] for a high speed (>100 Gbit/s) MB-OFDM direct-detection optical OFDM superchannel system with virtual carriers has been demonstrated as effective in MB-OFDM systems using DDO-OFDM, several challenges remain to be studied and investigation of their impacts when MB-OFDM signals are implemented in metro networks is required. Some challenges can be, for example, the type of electro-optic converter employed; the complexity of the edge node differs if the MB-OFDM signal assigned to each wavelength is totally extracted at a certain node or is shared over different nodes and also where the SSBI compensation is performed.

1.1.5 Memory polynomials

As it was referred in section 1.1.3, DDO-OFDM signals suffer from severe non-linear distortion (NLD) during the detection process, caused by the optical-electrical conversion. To mitigate the NLD, several solutions have been proposed [18-27] by mitigating the non-linearity of the transmission channel, S, with an approximate inverse system S^{-1}. In order to implement this S^{-1} system, different approaches have been proposed [19-21]. However, all these proposals were memoryless, which means that, the system S^{-1} only tries to compensate for the instantaneous non-linear behaviour of system S. With the increase of signal bandwidth, the impact of memory effects on system S non-linearities reduces the accuracy that can be obtained with the memoryless implementation of system S^{-1}. An alternative to increase the accuracy of the S^{-1} system implementation is using a digital distorter with memory, based on memory polynomials (MPs) [22-27]. One advantage of MP-methods is the flexibility to adapt on real-time to variations of the parameters of system S.

However, the implementations in [22-26] were developed for narrow-band radio frequency (RF) signals, applying the digital distortion to a baseband equivalent of the bandpass RF signal. In this approach, the MP-method used is called generalized memory polynomials (GMP), which reduces the sampling frequency requirements of the digital distorter when narrow-band signals modulate high frequency RF-carriers. For broadband signals, such as the ones that will be used in this work, where the signal bandwidth is comparable to the RF centre frequency, the reduction in the sampling frequency requirements is not that significant anymore. Also, to use GMP in this case, it is necessary to down-convert and up-convert the broadband signal at the input and output of the digital distorter. So, the alternative is to implement the digital distortion directly to the original signal, covering the whole band from DC up to the highest frequency of the signal.

In this dissertation, the implementation of a digital distorter employing memory polynomials is studied to mitigate the non-linear SSBI effect.

1.2 Motivation and objectives of the dissertation

The 100 Gb/s SSB MB-OFDM system which is intended to be implemented in metropolitan networks has major benefits thanks to the use of MB-OFDM signals. In order to benefit from those

advantages, while using direct-detection to lower the system cost and a dual parallel – Mach Zehnder modulator to easily create a SSB signal, it is imperative that the distortion originated at the receiver (SSBI) is mitigated. To do so, DSP algorithms are to be used, employing MP. Since MPs are not designed to specifically mitigate the SSBI, but instead mitigate any distortions that arise between the transmitter and the DSP, the motivation is to determine how far can this mitigation be performed and if it is possible to remove the SSBI distortion from the OFDM signal at the receiver.

To assess the performance of the MP algorithms implemented in the DSP to mitigate the SSBI, it is necessary to meet certain objectives, these objectives being:

i. Study and characterisation of MB-OFDM signals, in the time and frequency domain;
ii. Study and characterisation of the sub-systems of the MB-OFDM metro network;
iii. Study and characterisation of the MP theory;
iv. Study and characterisation of SSBI mitigation technique;
v. Identification of the minimum optical signal-to-noise ratio (OSNR) required to achieve a BER=10^{-3} in 100 Gb/s SSB MB-OFDM metro systems when SSBI mitigation using MP is employed.

1.3 Structure of the dissertation

The following 4 chapters and 2 appendixes are structured according to the objectives mapped in section 1.2.

In chapter 2, the introduction to optical OFDM is given. In this introduction the OFDM is defined mathematically alongside with its system description, advantages and disadvantages. The DDO-OFDM system is described and the demand for a SSB signal is presented. The optical modulator and photodetector are addressed and the SSBI that originates on the photodetector is introduced. At last, the MB-OFDM system is described and its parameters, considered in this work, are specified.

In chapter 3, the MP theory is presented and the MP structure considered in this work is described. The determination of the best structure to mitigate the SSBI is done. With the structure selected, it is presented an approach to help improve the scalability of the MP structure to any input OFDM sequence.

In chapter 4, four tests are conducted to assess the impact of a nonlinear band selector (2nd order super Gaussian) and of optical fibre on the system performance. In these tests, the MP structure chosen in chapter 3 is evaluated to determine if the MP is capable of mitigating the SSBI. These evaluations are performed to define the minimum required OSNR to achieve a BER of 10^{-3}.

In chapter 5, the final conclusions of the work developed are presented and suggestions of work to the future are presented.

In appendix A, some components of the simulator developed are described.

In appendix B, the results from the studied done on chapter 4 are presented.

1.4 Main original contributions

The main contributions of this dissertation when compared to other work developed are:

- Evaluation of the improvement achieved with digital post-compensation employing MPs to mitigate the SSBI in a DD SSB MB-OFDM system.
- Determination of the minimum required OSNR to achieve a BER of 10^{-3} when MPs are used to mitigate the SSBI in a DD SSB MB-OFDM system, with DP-MZM as optical modulator.

Chapter 2 - Principles of MB-OFDM

In this chapter, it is given an introduction to OFDM and to the SSB DDO-OFDM system. It is explained as well the MB-OFDM system and its parameters.

2.1 Basic principles of OFDM

When talking about modulation, there are two types, the single carrier modulation (SCM) and multicarrier modulation (MCM). OFDM belongs to the multicarrier group, the type of modulation that carries information data through many low rate subcarriers.

Since the year of 1966 [28] (year when the concept of OFDM was first introduced by Chang) OFDM has been used in many applications and standards like European DVB (Digital Video Broadcasting), wireless local area networks (Wi-Fi; 802.11a/g), wireless metropolitan area networks (WiMAX; 802.16e), asymmetric digital subscriber line (ADSL; ITU G.992.1) and long term evolution (LTE). The use of OFDM in optical communications occurred relatively late compared to the wireless communications.

2.1.1 Mathematical definition of OFDM

OFDM belongs to the MCM group. The generic implementation of an MCM system is represented in figure 2.1, which also includes the structure of an I/Q modulator/demodulator, commonly used in MCM systems.

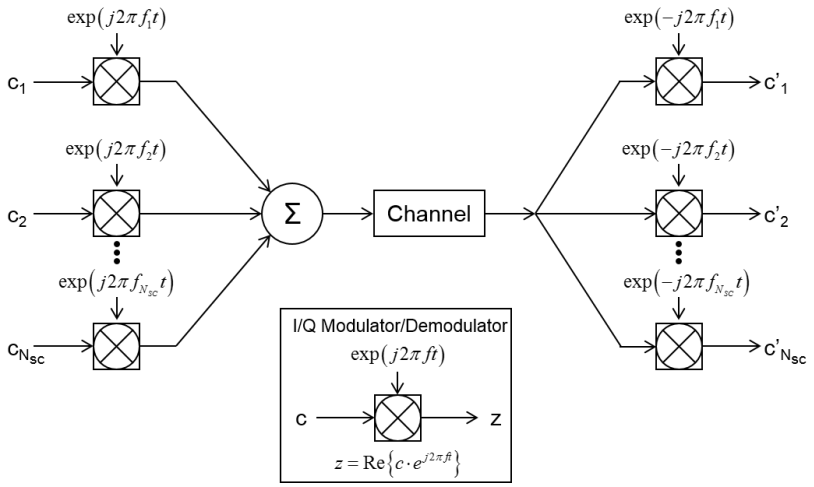

Figure 2.1 - General implementation of a MCM system.

A MCM signal with N_{sc} subcarriers and with a period per symbol of T_s can be represented by

$$s(t) = \sum_{i=-\infty}^{+\infty} \sum_{k=1}^{N_{sc}} c_{ki} s_k (t - iT_s) \tag{2.1}$$

where c_{ki} represents the ith information symbol at the kth subcarrier and s_k the waveform of kth subcarrier, defined by

$$s_k(t) = \Pi(t) e^{j2\pi f_k t} \tag{2.2}$$

where f_k is the frequency of the subcarrier and the $\Pi(t)$ represents the pulse shaping function, which is of rectangular form and is given by

$$\Pi(t) = \begin{cases} 1, & (0 < t < T_s) \\ 0, & (t \le 0, t > T_s) \end{cases}. \tag{2.3}$$

At the receiver end of a MCM system, the demodulation of the signal can be executed using a filter (one filter to each subcarrier waveform) or using a correlator (matched to the subcarrier). Since classical MCM uses non-overlapped band-limited signals, which can be implemented using a bank containing a large number of oscillators and filters at both transmitter and receiver [29-30], this represents the biggest disadvantage of MCM because it requires excessive bandwidth. A good and recent solution to overcome this problem is using overlapped signals. This solution is called OFDM. The concept of orthogonality between sub-carriers to achieve high-spectral efficiency transmission was proposed in [29]. This orthogonality originates from the correlation between two subcarriers, given by

$$\langle s_k, s_l \rangle = \frac{1}{T_s} \int_0^{T_s} s_k s_l^* dt = \frac{1}{T_s} \int_0^{T_s} e^{(j2\pi(f_k - f_l)t)} dt = e^{(j\pi(f_k - f_l)T_s)} \frac{\sin(\pi(f_k - f_l)T_s)}{\pi(f_k - f_l)T_s}. \tag{2.4}$$

It can be seen that if the condition

$$f_k - f_l = m \frac{1}{T_s} \tag{2.5}$$

where f_k and f_l are the frequencies of each subcarrier, m is an integer (which indicates for example for m=1 that f_k and f_l are adjacent) and T_s is the symbol period, is verified, then it means that two subcarriers are orthogonal. More specifically, two sets of orthogonal subcarriers, with their frequencies spaced at multiple of the inverse of the symbol period can be recovered using matched filters, avoiding inter-carrier interference (ICI).

2.1.2 Inverse fast Fourier transform

Transmitting an OFDM signal is very demanding and complex. This happens because it requires, at the transmitter and receiver's end, a bank containing a large amount of modulators and filters to generate the orthogonal subcarriers.

The solution found to solve this problem was that OFDM modulation/demodulation could be implemented by using inverse discrete Fourier transform (IDFT)/discrete Fourier transform (DFT) [31].

To prove this, first consider the mth sample of $s(t)$ from the equation 2.1

$$s_m = \sum_{k=1}^{N_{sc}} c_k e^{j2\pi f_k \frac{(m-1)T_s}{N_{sc}}}. \tag{2.6}$$

Then, using the orthogonally condition of equation 2.5 and assuming that

$$f_k = \frac{k-1}{T_s} \tag{2.7}$$

the result of substituting equation 2.7 in equation 2.6 is

$$s_m = \sum_{k=1}^{N_{sc}} c_k e^{j2\pi f_k \frac{(m-1)T_s}{N_{sc}}} = \sum_{k=1}^{N_{sc}} c_k e^{j2\pi \frac{(k-1)(m-1)}{N_{sc}}} = \mathrm{IDFT}\{c_k\} \tag{2.8}$$

where IDFT is the inverse discrete Fourier transform and $m \in [1, N_{sc}] \cap \mathbb{N}$. The similar process can be executed at the receiver end, in which the result is

$$c_k^{'} = \mathrm{DFT}\{r_m\} \tag{2.9}$$

where r_m is the discrete value of the received OFDM signal $r(t)$.

The usage of IDFT/DFT in the transmission of an OFDM signal brings two advantages. The first one being the fact that the IFFT/FFT (Inverse Fast Fourier Transform/Fast Fourier Transform) algorithm is efficient, because the number of complex multiplications are reduced from N_{sc}^2 to almost linearly with the number of subcarriers N_{sc} [32]. The second advantage is the fact that a great number of orthogonal subcarriers can be created without needing complex RF oscillators and filters. This leads to a simple architecture system, which will be presented in section 2.6.

2.1.3 Cyclic prefix

The transmission of an OFDM signal, across a fiber link, is affected by two interferences, the ISI (interference between consecutive symbols) and ICI (interference between subcarriers, within the same symbol). These two negative effects are caused, respectively, by the dispersive channel and the frequency offset of the subcarriers.

To solve the problem with ISI, the technique used is to leave a gap between OFDM symbols, by extending each OFDM symbol with a guard band interval. Since the problem with ISI is the fact that the dispersive delay makes a symbol to overlap its adjacent symbol, therefore, in order to ISI to be completely suppressed, the guard band interval has to be bigger than the dispersive delay, resulting in

$$t_d < \Delta_G \tag{2.10}$$

where t_d is the delay spread of an OFDM symbol and Δ_G is the guard band interval.

Despite the fact that the guard band technique solves the ISI problem, the ICI effect remains unsolved. In order to solve this, the cyclic prefix (CP) needs to be used. CP was proposed to solve both ISI and ICI [33]. When CP is used, the last samples of each OFDM symbol are replicated and added to the beginning of the OFDM symbol. With the addition of the samples, which make the symbol carry an amount of information twice, the transmission efficiency is reduced. Therefore the CP needs to be as small as possible.

The following example contains two consecutive OFDM symbols, where it will be applied CP. In figure 2.2 A, the two OFDM symbols are in an ideal channel. Then in figure 2.2 B, the channel is dispersive, which will add a delay spread to the first OFDM symbol, resulting in the overlapping with the neighbor OFDM symbol. This leads to ISI. Additionally, this will lead to ICI because, since the waveform inside the DFT window no longer has a complete OFDM symbol, the orthogonality condition between

subcarriers is lost. To solve this, in figure 2.2 C, the CP is implemented by cyclic extension of the OFDM waveform into the guard band interval. Finally, in figure 2.2 D, it is possible to observe that by introducing the CP and ensuring that the delay spread is smaller than guard band interval, a complete OFDM symbol

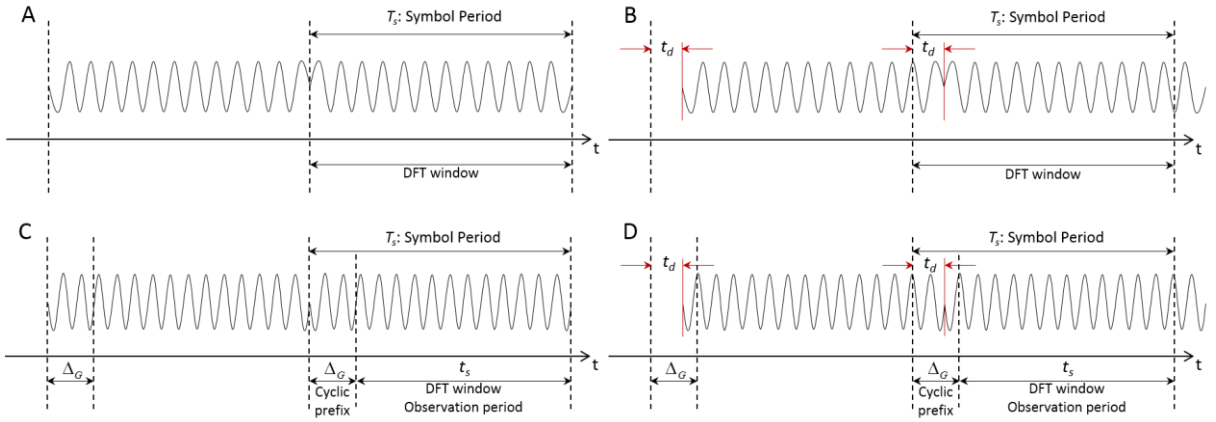

Figure 2.2 - (A) ideal channel, (B) dispersive channel without CP, (C) dispersive channel with CP at the transmitter side, (D) dispersive channel with CP at the receiver side.

is inside the DFT window. This happens because, although the channel is dispersive and adds a delay spread, since the delay is smaller than the guard interval, the portion of OFDM symbol that was shifted out of the window is assured by the CP. As such, the OFDM symbol is almost an identical copy of the transmitted one, with an additional phase shift. This phase shift is dealt with through channel estimation and will be consequently removed for symbol decision.

With the introduction of CP, the expressions presented at the beginning of this chapter need to be changed. But, to maintain the equation 2.1 for the transmitted signal, the pulse shaping function 2.3 needs to be rewritten as

$$\Pi(t) = \begin{cases} 1, & (-\Delta_G < t \le T_s) \\ 0, & (t \le -\Delta_G, t > T_s) \end{cases}. \tag{2.11}$$

2.1.4 I/Q modulator

A baseband OFDM signal is, in general, in the complex form. Therefore, it needs to be up-converted for transmission purposes, in order to convert the complex value into a real one.

The hardware involved in this conversion is a complex multiplier (mixer) or IQ modulator/demodulator, similar to the one represented in figure 2.3.

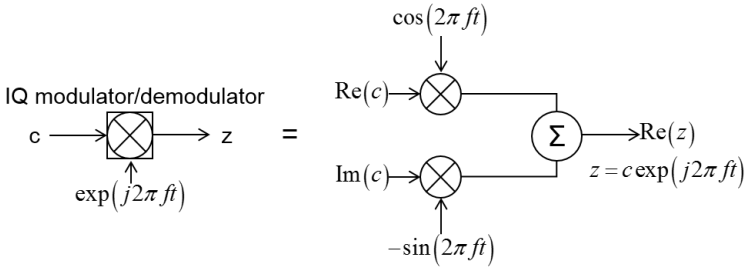

Figure 2.3 - Representation of an IQ modulator for up-conversion of a baseband complex value c to passband real value z.

The real valued signal at the output of the IQ modulator is given by

$$s_{RF}(t) = \mathrm{Re}\left\{s(t)e^{j2\pi f_{RF}t}\right\} = \mathrm{Re}\left\{s(t)\right\}\cdot\cos(2\pi f_{RF}t) - \mathrm{Im}\left\{s(t)\right\}\cdot\sin(2\pi f_{RF}t) \quad (2.12)$$

where $s_{RF}(t)$ is the passband real-valued signal, which is centred at the frequency f_{RF} and $s(t)$ is the baseband complex value, composed by its real and imaginary components. In appendix A.3, it is explained in more detail the process of up and down-conversion.

2.1.5 OFDM system description

Figure 2.4 shows a simple block diagram of an OFDM transmitter and receiver.

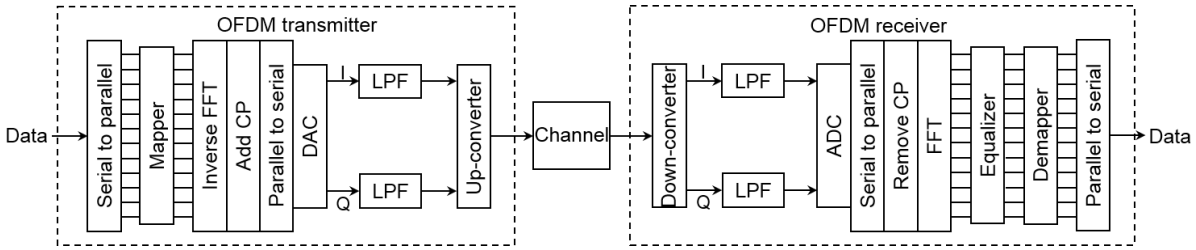

Figure 2.4 - Block diagram of an OFDM system.

Starting at the transmitter, the OFDM signal is created in the following sequence:

- The input bit serial stream enters the serial to parallel converter (S/P) where it is splitted into N_{sc} parallel bit streams;

- Then each of these bit streams is mapped into a symbol stream using for example a M-ary quadrature amplitude modulation (M-QAM);

- Afterwards, the recently mapped symbols enter the IFFT where they are converted into an OFDM symbol stream;

- To prevent occurrence of ISI and ICI the cyclic prefix is added to each one of the OFDM symbols;

- Then, at the parallel to serial (P/S) converter, the OFDM symbols are converted to a serial data stream, in which the I/Q components of the signal are separated into independent channels. After that, these components are converted from digital to the analogue form at the digital-to-analogue converter (DAC), which is explained in more detail in appendix A.1;

- While being in independent channels, after converted to analogue, each I/Q component is filtered (filter with the bandwidth of the OFDM signal), in order to attenuate or remove the distortions created by the DAC.

- At last, the I/Q components enter the up-converter where they are combined and up-converted to the carrier frequency, in order to generate the OFDM signal that will be sent to the channel.

When the OFDM signal reaches the receiver, its process is the same of the transmitter but backwardly, with the addition of a single-tap equalizer block next to the FFT. The equalizer uses training symbols to estimate the channel characteristic, in order to compensate the distortion caused by the transmission channel. The channel estimation, done in the equalizer, is described in more detail in appendix A.4.

2.1.6 Spectral efficiency of an OFDM signal

One of the major advantages of OFDM is its high spectral efficiency. This happens because, since OFDM uses overlapped orthogonal subcarriers, they occupy less bandwidth. Before starting to demonstrate how OFDM spectral efficiency is defined, the first thing to do is to present the OFDM frame, which is represented in figure 2.5. The frame is represented in time and frequency, including the N_{sc} subcarriers in frequency and the total number of OFDM symbols N_S. The total number of OFDM symbols is composed by the training symbols (N_{ts}), which are used for channel estimation and data symbols (N_{ds}), responsible for carrying the information data.

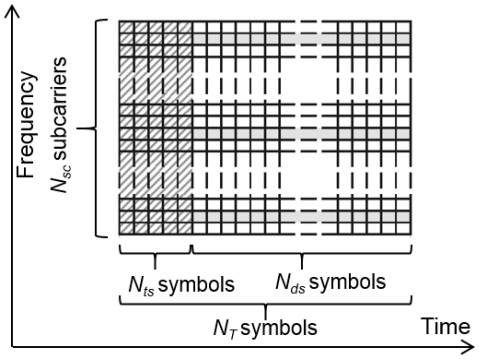

Figure 2.5 - Representation of an OFDM frame.

Then, to define the OFDM spectral efficiency, it is first considered an ideal OFDM system with no guard interval, Δ_G, and with all N_{sc} subcarriers carrying data. The corresponding bitrate is defined by

$$R_b = \frac{N_{sc}}{T_s}\log_2 M \tag{2.13}$$

where T_s represents the OFDM symbol period and M the number of different symbols of the modulation scheme. After this, it is necessary to add the guard interval and the training symbols, which will reduce the bitrate. Therefore, the real bitrate is given by [33-34]

$$R_b = \frac{N_{ds}N_{sc}\log_2 M}{N_s T_s} = \frac{N_{ds}N_{sc}\log_2 M}{(N_{ds}+N_{ts})(t_s+\Delta_G)}. \tag{2.14}$$

In equation 2.14 $T_s = t_s + \Delta_G$, where t_s is the DFT window observation period. Since M represents the number of different symbols of the modulation scheme, then, $\log_2 M$ represents the number of bits per subcarrier. The bandwidth of an OFDM signal is illustrated in figure 2.6 and is defined as [34]

$$B_{OFDM} = \frac{2}{T_s} + \frac{N_{sc}-1}{(T_s-\Delta_G)} \tag{2.15}$$

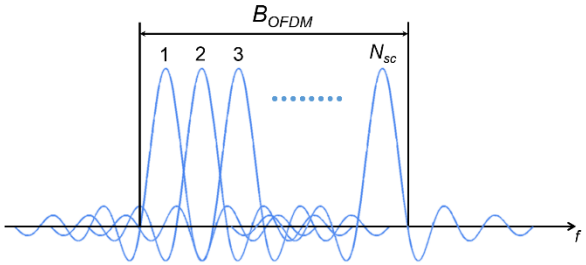

Figure 2.6 - Representation of the bandwidth of an OFDM symbol.

The spectral efficiency of an OFDM signal (η_{spt}) is the ratio between the bitrate and the bandwidth

$$\eta_{spt} = \frac{R_b}{B_{OFDM}} \tag{2.16}$$

in which, by substituting equation 2.14 and 2.15 on equation 2.16, the spectral efficiency is given by

$$\eta_{spt} = \frac{\left(1-\alpha_G\right)}{2\left(1-\alpha_G\right)+N_{sc}-1} \cdot \frac{N_{ds}N_{sc}}{N_s} \cdot \log_2 M. \tag{2.17}$$

Analysing the equation 2.18, there are two ways of improving the spectral efficiency of an OFDM system. On one hand, it can be improved by using an high-order modulation scheme. On the other hand, it can be improved by reducing the guard interval and the number of training symbols. Although equation 2.17 gives the correct value for the spectral efficiency, in this work it will be considered a more simplified version of this equation given by

$$\eta_{spt} = \log_2 M \tag{2.18}$$

This simplification is achieved by considering that the number of OFDM symbols is approximately equal to the number of OFDM information symbols and that the guard interval factor is approximately zero.

2.1.7 Disadvantages of OFDM

One of the major disadvantages of OFDM modulation format is the high peak-to-average power ratio. PAPR is the ratio between the maximum power of a sample in a given OFDM symbol and the average power of that OFDM symbol, given by

$$PAPR = \frac{\max\left\{\left|s(t)\right|^2\right\}}{E\left\{\left|s(t)\right|^2\right\}}, t \in \left[0, T_s\right]. \tag{2.19}$$

PAPR occurs when, in a multicarrier system, the different subcarriers are out of phase with each other. When all the subcarriers achieve the maximum value simultaneously, this will cause the output envelope to suddenly shoot up which causes a 'peak' in the output envelope. Due to presence of large number of independently modulated subcarriers in an OFDM signal, the peak value of the OFDM signal can be very high as compared to the signal average power. PAPR reduction can be achieved through algorithms without compromising bandwidth efficiency or computer complexity.[35]

Other two disadvantages of OFDM are the frequency offset and the phase noise sensitivity. Both frequency offset and phase noise lead to ICI, because, since OFDM belongs to the multicarrier modulation group, its symbol period is much longer than the single carrier symbol [13, 35-39].

Frequency offset can be mitigated through frequency estimation and compensation, and phase noise sensitivity through the design of RF local oscillators that satisfy the required phase noise specification. The phase noise problem is very important to optical OFDM. This happens because, although several studies have been focused on designing lasers with low laser linewidth, the laser phase noise is often relatively large. The impact of laser phase noise is very critical especially when using high order constellations to achieve high spectral efficiency modulation [40].

2.2 Direct detection optical OFDM

2.2.1 Direct detection optical OFDM system description

In chapter 1, it was introduced the direct-detection optical OFDM system. The key feature of a DDO-OFDM is that it only needs a photodetector at the receiver, which is less expensive and complex when compared to the CO-OFDM system. A generic diagram of a DDO-OFDM system is represented in figure 2.7.

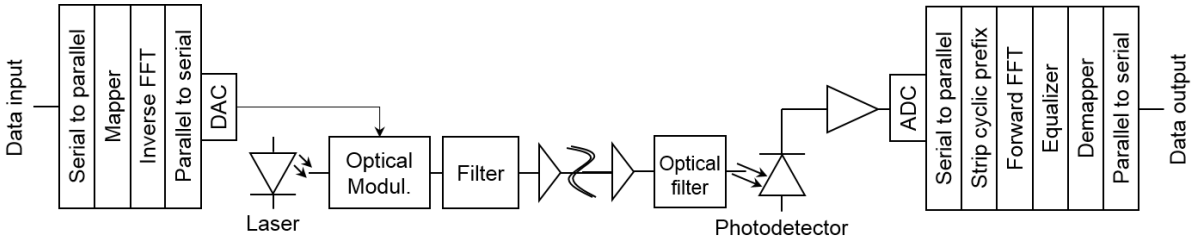

Figure 2.7 - Representation of the DDO-OFDM system.

The system description is similar to the one presented in section 2.1.5. In this dissertation, the signal used is a single-sideband OFDM signal, which is going to be introduced in section 2.2.2; the optical modulator used is a dual-parallel Mach-Zehnder modulator, presented in section 2.2.3 and the photodetector used is a positive-intrinsic-negative (PIN) photodiode described in section 2.2.4. In section 2.2.5, mitigation techniques to the distortion introduced in section 2.2.4 are presented.

2.2.2 Single-sideband DDO-OFDM

Metro networks are impaired by chromatic dispersion induced power fading (CDIPF). Figure 2.8 A represents the signal at the input and output of the PIN photodetector, where it is illustrated the effect of the CDIPF. This power fading appears because of the destructive beat between the two sidebands, which is caused by the square law characteristic of the PIN and caused by the accumulated chromatic dispersion of the fibre link.

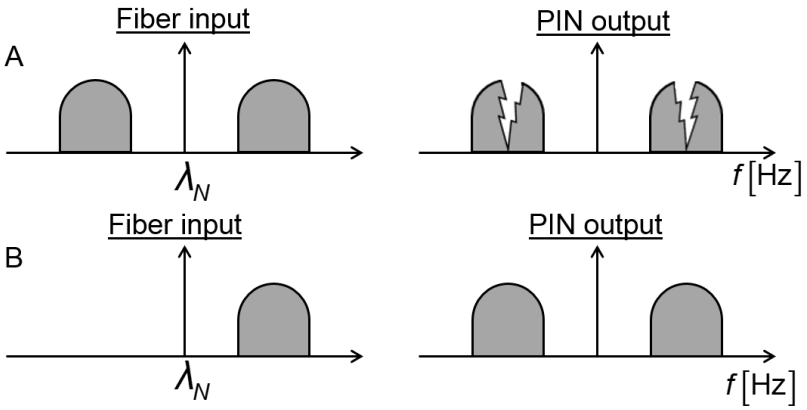

Figure 2.8 - Illustration of the CDIPF effect on (A) the double sideband OFDM signal and (B) the SSB OFDM signal.

To overcome the CDIPF, there are two techniques that may be used, single side band (SSB) transmission and optical dispersion compensation. The SSB technique consists in transmitting only one of the two sidebands, making it possible to avoid the beat interference at the PIN (represented in figure

2.8 B). The other technique is used to remove all the chromatic dispersion in order to avoid the destructive beat between the two sidebands. The main difference between these techniques is the part of the system where they are implemented. While SSB is implemented at the transmitter, optical dispersion compensation involves installing blocks of dispersion compensating fibre through the fibre link. Nowadays, network operators are working on moving all the network design to the transmitter and receiver's side, in order to leave the fibre links intact. So, if an upgrade is developed, it is no longer necessary to modify the fibre links. Therefore the SSB technique is more suitable.

SSB OFDM has been widely proposed alongside systems employing DDO-OFDM. These SSB DDO-OFDM systems require a frequency gap between the optical frequency carrier and the OFDM signal. The frequency gap has usually the same width as the OFDM signal bandwidth and it is necessary to accommodate the distortion induced by the SSBI term generated by the photodetector.

2.2.3 Dual-parallel Mach-Zehnder modulator

The creation of a SSB-OFDM signal can be achieved by using an optical filter. However, the usage of an optical filter has several disadvantages, for instance, loss of power in the optical carrier, distortion on the remaining sideband, cross-talk caused by the residual sideband and reduced spectral efficiency, caused by the gap between the optical carrier and the OFDM information sideband, required for a correct filtering of the residual sideband. Another device capable of creating the SSB-OFDM signal, which does not suffer from the disadvantages listed above, is the dual-parallel Mach-Zehnder modulator (DP-MZM), proposed in [41].

The structure of the DP-MZM is represented in the figure 2.9 and consists in a MZM with a MZM inserted in each arm. Since MZMs are composed by two parallel phase modulators, then this leads to a four phase-modulator structure.

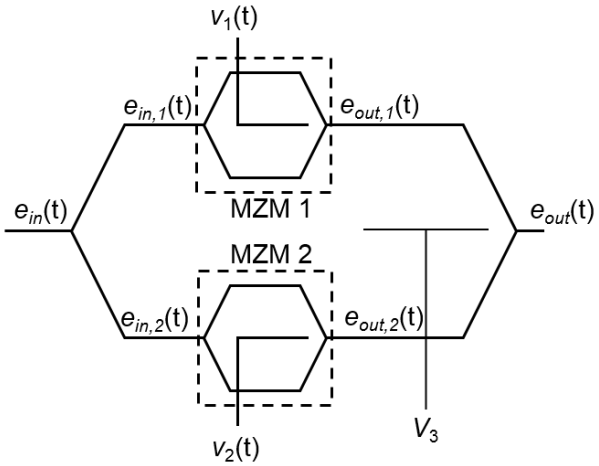

Figure 2.9 - Illustration of a DP-MZM.

By observing figure 2.9, it can be seen that when the signal enters the DP-MZM it is splitted into the two arms of the modulator. Additionally, a signal is created in each arm and then, the third modulator is used to put the two signals in quadrature to each other.

The input-output characteristic of a DP-MZM, $C_{i,o}$, is given by [40]

$$C_{i,o}(t)=\frac{e_{out}(t)}{e_{in}(t)}=\left[\frac{1}{2}\exp\left(j\pi\left(-\frac{V_3}{2V_{sv}}\right)\right)C_{i1,o1}(t)+\frac{1}{2}\exp\left(-j\pi\left(-\frac{V_3}{2V_{sv}}\right)\right)C_{i2,o2}(t)\right] \quad (2.20)$$

where $e_{in}(t)$ is the optical field at the input and $e_{out}(t)$ the optical field at the output of the DP-MZM and V_{sv} is the switching voltage, which represents the voltage between the maximum and minimum of power. The $C_{i1,o1}$ and $C_{i2,o2}$ are the input-output characteristics of MZM1 and MZM2 and are given by

$$\begin{aligned} C_{i1,o1}(t)&=\frac{e_{out,1}(t)}{e_{in,1}(t)}=\cos\left(\frac{\pi}{2V_{sv}}\left[v_1(t)-V_{b1}\right]\right)\\ C_{i2,o2}(t)&=\frac{e_{out,2}(t)}{e_{in,2}(t)}=\cos\left(\frac{\pi}{2V_{sv}}\left[v_2(t)-V_{b2}\right]\right)\end{aligned} \quad (2.21)$$

where $e_{in,1}(t)$ and $e_{in,2}(t)$ are the optical fields at the input of MZM1 and MZM2; $e_{out,1}(t)$ and $e_{out,2}(t)$ are the optical fields at the output of MZM1 and MZM2 and V_{b1} and V_{b2} are the switching voltages of MZM1 and MZM2. The DP-MZM can be biased in many different ways. The two most common are the quadrature bias point and the null bias point. On both ways, the outer MZM is always biased at the quadrature point ($V_3 = V_{sv}/2$), resulting in a phase difference of 90º between MZM1 and MZM2 outputs. On one hand, the inner MZMs can be biased at the quadrature point ($V_{b1} = V_{b2} = V_{sv}/2$). In this case the, equation 2.20 is simplified to

$$C_{i,o}(t)=\frac{e_{out}(t)}{e_{in}(t)}=\frac{1}{2}\left[\exp\left(-j\frac{\pi}{4}\right)\cos\left(-\frac{\pi}{4}+\frac{\pi}{2V_{sv}}v_1(t)\right)+\exp\left(j\frac{\pi}{4}\right)\cos\left(-\frac{\pi}{4}+\frac{\pi}{2V_{sv}}v_2(t)\right)\right] \quad (2.22)$$

On the other hand, the inner MZMs can be biased at the null point. To achieve this case, $V_{b1} = V_{b2} = V_{sv}$. In this case, the equation 2.20 can be simplified to

$$C_{i,o}(t)=\frac{e_{out}(t)}{e_{in}(t)}=\frac{1}{2}\left[\exp\left(-j\frac{\pi}{4}\right)\cos\left(-\frac{\pi}{2}+\frac{\pi}{2V_{sv}}v_1(t)\right)+\exp\left(j\frac{\pi}{4}\right)\cos\left(-\frac{\pi}{2}+\frac{\pi}{2V_{sv}}v_2(t)\right)\right]. \quad (2.23)$$

In order to generate the SSB-OFDM signal, the OFDM signal and its Hilbert transform (HT) need to be applied to the electrical arms of the DP-MZM [42]. Considering figure 2.9, $v_1(t)$ represents the OFDM signal and $v_2(t)$ the Hilbert transform of the OFDM signal. Each of these signals are related to the switching voltage, V_{sv}, through the modulation index, m. The equation of the modulation index is given by

$$m=\frac{V_{RMS,(1,2)}}{V_{sv}}\times 100 \quad where \quad \begin{aligned} V_{RMS,1}&=\sqrt{\left\langle\left|v_1(t)\right|^2\right\rangle}\\ V_{RMS,2}&=\sqrt{\left\langle\left|v_2(t)\right|^2\right\rangle}\end{aligned}. \quad (2.24)$$

Then, the bias point of the inner MZMs depends on the type of SSB-OFDM signal that is needed. If a carrier-suppressed SSB-OFDM signal is needed, the inner MZMs must be biased at the null point. If the carrier of the SSB-OFDM signal does not need to be suppressed, then the inner MZMs may be at the quadrature point [5]. The electro-optic conversion performed by the DP-MZM is a non-linear operation. This can be verified by the presence of a cosine function in the equation belonging to the two bias cases presented before. Since this non-linear effect increases with the increase of the electrical signal voltage

applied to the DP-MZM, it should be lowered. However, if it is lowered, then the signal-to-noise ratio (SNR) is lowered as well. In conclusion, there should be defined a reasonable voltage value that represents a good compromise between SNR and the non-linear effects introduced by the modulator.

2.2.4 Positive-intrinsic-negative photodetector

After the SSB-OFDM signal is created, it travels through the optical fibre, which adds chromatic dispersion. When it reaches the receiver's end, the signal is converted from optical to the electrical domain in the photodetector, usually a PIN. The following deduction shows how the SSBI appears. After the photodetection, the PIN output current $i_{pin}(t)$ is given by

$$i_{pin}(t) = R_{\lambda} \times p_{pin}(t) \tag{2.25}$$

where $p_{pin}(t)$ is the optical power of the incident optical signal and R_{λ} the PIN responsivity. In this situation, the instantaneous power of an optical signal at the PIN input is given by

$$p_{pin}(t) = \left| e_{pin}(t) \right|^2 \tag{2.26}$$

where $e_{pin}(t)$ is the optical field at the PIN input. To maintain the simplicity of this deduction, the output of the E/O is considered to be directly connect to the PIN input. Therefore, the optical field at its input is given by

$$e_{pin}(t) = A + Bs(t) \tag{2.27}$$

where A is a constant proportional to the optical carrier, B is a constant that depends of V_{sv} and $s(t)$ is the OFDM signal from equation 2.1. Using equation 2.27 in 2.26 and considering that A and B are real, we obtain

$$i_{pin}(t) = R_{\lambda} \cdot \left| e_{pin}(t) \right|^2 = R_{\lambda} \left[A^2 + 2ABs(t) + B^2 s^2(t) \right]. \tag{2.28}$$

In equation 2.28, the first term is the DC component A^2, the first order component $2ABs(t)$ is the received OFDM signal and the second order component $B^2s^2(t)$ is a nonlinear product, also known as signal-signal beat interference (SSBI), that may induce degradation on the detected electrical OFDM signal at the receiver end. In figure 2.10, it is an illustration of the SSBI distortion.

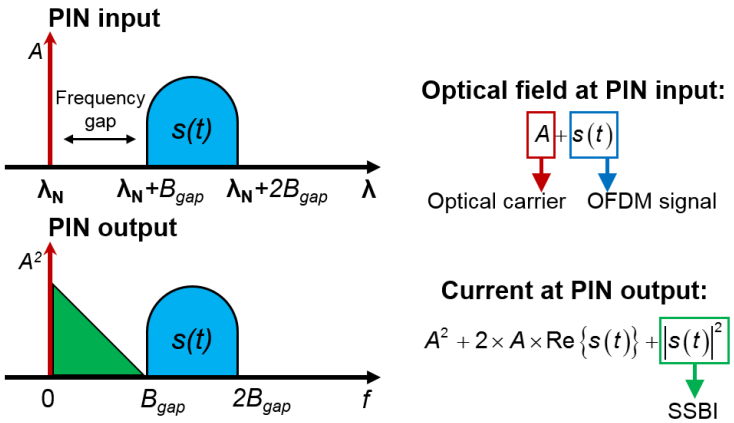

Figure 2.10 - Illustration of the SSBI distortion.

2.2.5 SSBI mitigation techniques

As introduced in section 2.2.4, the SSBI is originated during the photodetection. Since the bandwidth of the SSBI is equal to the bandwidth of the OFDM band, after photodetection, the SSBI "appears on top" of the OFDM bandwidth, as shown in figure 2.10, adding distortion to the signal. Although there is a band gap (VBG) between the band and the VC, this gap is smaller than the SSBI bandwidth and it is not enough to accommodate the SSBI.

The following two architectures of transmitter and an iterative cancelation receiver are used to minimize the effect of the SSBI, induced by the PIN [6, 43, 44, 22-27].

2.2.5.1 Offset SSB-OFDM

The offset OFDM is proposed in [6] and the proof-of-concept experiment was demonstrated in [45] with the proposed system represented in figure 2.11. This system allocates, at the transmitter, a guard band between the optical carrier and the OFDM signal, to accommodate the second-order distortion term.

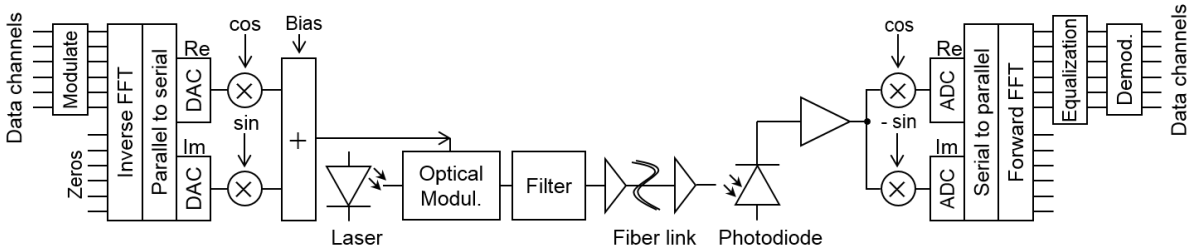

Figure 2.11 - Offset SSB OFDM system representation [45].

When the signal is photodetected at the receiver end, the RF spectrum obtained at the photodetector output has in the guard band the first and third terms of equation 2.28, more specifically the DC and SSBI components, and out of the guard band the OFDM signal spectrum. Therefore, the SSBI component does not overlap the OFDM signal, which means that it does not cause detrimental effects after electrical filtering. The downside of this system is the low spectral efficiency, since there must be a gap equal to the signal bandwidth between the optical carrier and the OFDM signal.

2.2.5.2 RF-tone assisted OFDM

RF-tone assisted OFDM is proposed in [43] and ought's to solve the major problem of the offset SSB OFDM system transmitter architecture, which is the low spectral efficiency. The RF-tone system, presented in figure 2.12, has two variations: the OFDM-A and OFDM-B. The first variation has a gap, with the same size as the OFDM spectrum, between the RF tone and the OFDM signal. The second variation only transports data in the odd subcarriers relative to the RF tone, leaving the even subcarriers empty. In both variations, the electrical OFDM signal after the IFFT is complex and is fed into an I/Q modulator.

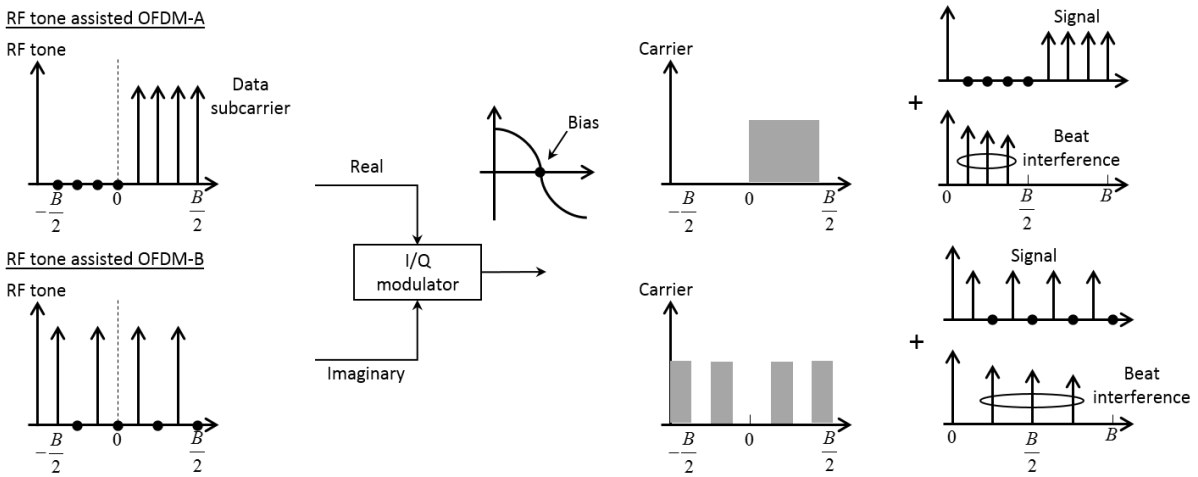

Figure 2.12 - RF tone-assisted OFDM system representation [43].

When comparing the OFDM-A with the offset SSB-OFDM in terms of bandwidth gap, considering *B* the total OFDM bandwidth, the RF tone in OFDM-A is B/2 away from the OFDM band, which is similar to the gap on the offset SSB OFDM. However, in OFDM-A there is no electrical RF up-conversion, which requires a smaller electrical bandwidth for the modulator.

After photodetection, the second order term of equation 2.28 is on the subcarriers of the gap, for OFDM-A and on the subcarriers interleaved with the data subcarriers for OFDM-B. This means that the data transferred in both OFDM-A and OFDM-B can be extracted without suffering from SSBI distortion effects.

2.2.5.3 SSBI cancelation receiver

In [44] it is proposed an iterative SSBI estimation and cancelation technique to be implemented at the receiver. With this technique it is possible to estimate the SSBI component using DSP algorithms. Then the estimated SSBI component is used to supress the SSBI at the receiver, reducing the frequency gap between the optical carrier and the OFDM band. Its working concept is represented in figure 2.13.

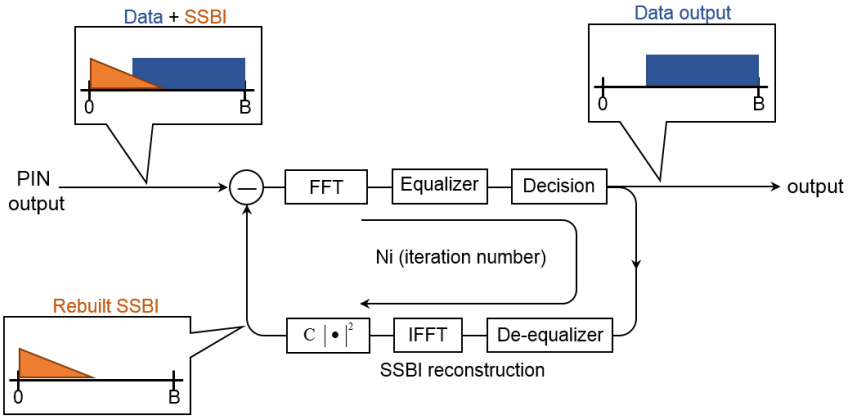

Figure 2.13 - SSBI cancelation receiver system diagram [44].

The block of the SSBI cancelation receiver is implemented between the PIN photodiode and the output. This iterative technique works as explained in the following: (1) The signal with the distortion is processed and used for hard decisions (decisions with errors); (2) then the recovered data is used to reconstruct the second-order distortion; and (3) the reconstructed distortion is subtracted from the original signal. To achieve a satisfactory result, this procedure needs to be executed many times, resulting in additional computer complexity.

2.3 Multiband-OFDM system

2.3.1 MORFEUS project

This dissertation is performed under the scope of the MORFEUS project [5]. The main objective of this project is to implement a metro network based on high data-rate MB-OFDM signals employing direct detection. This represents a great solution to provide, simultaneously, high flexibility in capacity allocation, high spectral efficiency and the possibility of upgrading the network capacity without changing the system architecture.

In this section, the concept of MB-OFDM is explained, the description of the MB-OFDM signal (used in the MORFEUS project) and MORFEUS node is performed.

2.3.2 Multiband-OFDM concept description

Multiband-OFDM uses multiple bands instead of a single-band, more specifically, it is based on the division of a WDM channel (ch_j) into several independent OFDM sub-bands ($b_{i,j}$) [46]. Each one of these sub-bands is an independent OFDM signal with its own optical carrier (FC_{ij}), as shown in figure 2.14.

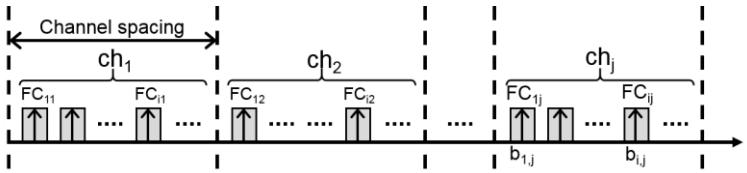

Figure 2.14 - Optical spectra of MB-OFDM signal.

2.3.3 Multiband-OFDM signal

In section 2.2.2, it was introduced the solution to CDIPF, which was using a SSB signal. It was also introduced in chapter 2.2.2, the SSBI problem, which could be mitigated by leaving a frequency gap between the frequency carrier and the OFDM signal. Therefore the MB-OFDM signal used in MORFEUS network should be a SSB MB-OFDM with a frequency gap, as illustrated in figure 2.15.

But, in order to accommodate the SSBI, the bandwidth of the frequency gap should be equal to the bandwidth of the OFDM signal. To determine the correct size of the gap bandwidth, it is important to understand how the detection process associated with a MB-OFDM signal is performed.

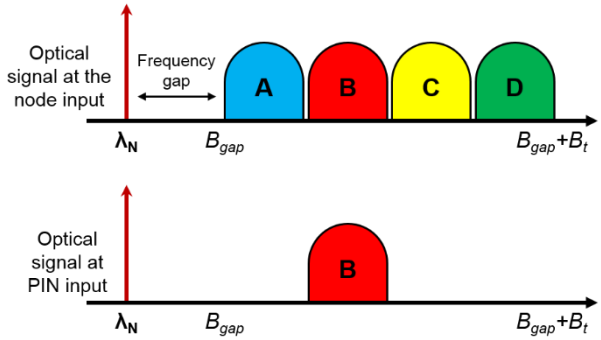

Figure 2.15 - Schematic illustration of the SSB MB-OFDM signal transmitted in the metro ring.

The simplest way is to photodetect all the bands presented in the signal. If the bandwidth of the SSB MB-OFDM signal is B_t, as depicted in figure 2.16, then the bandwidth of the frequency gap needs to be B_t as well, resulting in a huge electrical bandwidth requirement. This represents a problem on the networking aspect, because not all bands go to the same destination node. Therefore, only the band that is assigned to the node should be photodetected.

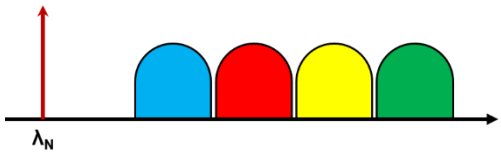

Figure 2.16 - Schematic illustration of the SSB MB-OFDM signal with a frequency gap similar to the one occupied by all the OFDM bands.

One method to detect only one band, instead of the entire SSB MB-OFDM signal, is the use a dual band optical filter. This filter needs to be a dual band because it needs to select the band that is assigned to the edge node and also the optical carrier of the signal that is being photodetected [17]. This solution is represented in figure 2.17, where the band B is being photodetected.

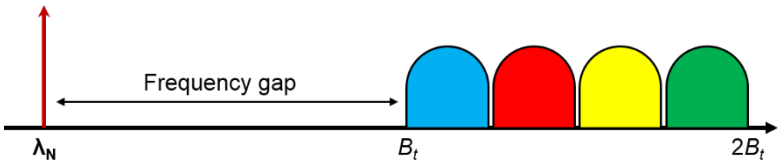

Figure 2.17 - Schematic illustration of the SSB MB-OFDM signal with a frequency gap similar to the one occupied by one OFDM band.

In this example, the size of the bands is considered to be the same. If the bands were of different bandwidths, the frequency gap should have the same bandwidth as the band that is being photodetected. Although this method of photodetection increases the spectral efficiency when compared to the photodetection of the entire signal, it still is not very effective because if the OFDM band that is to be photodetected has the highest central frequency (for example band D from the figure 2.17), then the receiver still needs to have a bandwidth much bigger than the OFDM band, resulting in a waste of resources. Another disadvantage of the dual band filter is developing a filter capable to perform the selection of each band, not because of the nature of the filter, but because of the high selectivity needed to select only one band and discard all the others to produce as low cross-talk as possible. They also

need to be dynamically adjustable, because the band that needs to be photodetected depends on the edge node that it is assigned to. Nowadays, these filters are very complex to develop and very expensive to acquire. In conclusion, all this disadvantages make the dual band filter an unreliable solution to implement.

Another method to only detect one OFDM band is to use a virtual carrier close to each OFDM band to assist in the detection process of that band. The use of virtual carriers has been proposed in different works in the past few years [47-49]. In this case, the virtual carrier is generated in the electrical domain, alongside each OFDM band, resulting in the SSB MB-OFDM signal represented in figure 2.18 a). When the signal arrives at an edge node, a conventional optical filter is used to select the correct OFDM band, and its corresponding virtual carrier, to be photodetected, as represented in figure 2.18 b).

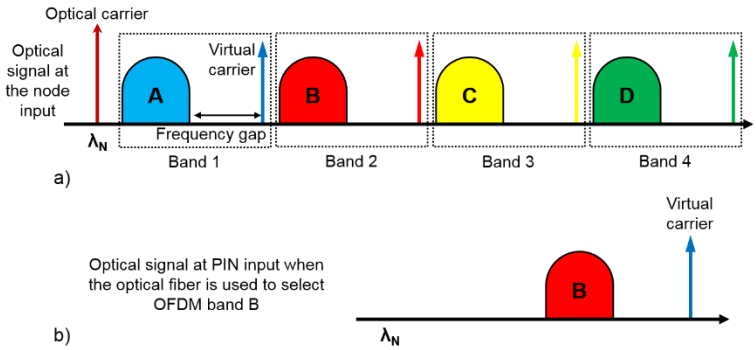

Figure 2.18 - a) SSB MB-OFDM optical signal with virtual carriers at the input of each node. b) SSB MB-OFDM optical signal with virtual carriers at the PIN input when an optical filter is used to select OFDM band B.

Although the use of virtual carriers allows to bypass the use of a dual band filter, it does not increase the spectral efficiency because of the frequency gap between the OFDM band and the corresponding virtual carrier, as demonstrated in figure 2.18 a). Therefore, the only way to increase the spectral efficiency is reducing the frequency gap, which would also reduce the bandwidth constraints of the receiver front-end and its analogue-to-digital converters. However, the reduction in the frequency gap leads to an increase of the signal distortion caused by the SSBI. To reduce this impact, there two approaches. One is to increase significantly the power of each virtual carrier compared to the power of the corresponding OFDM band. This method allows the PIN output current to be dominated by the beat between the carrier and the OFDM, which reduces the impact of the SSBI distortion on the received OFDM signal. However, it also increases the optical-to-signal noise ratio (OSNR) needed to achieve a certain value for the bit-error-ratio (BER). Another approach is to implement DSP algorithms at the receiver end in order to reconstruct the SSBI term and remove it from the photodetected signal. Although this method increases the system complexity, the advantages provided by this technique and the recent advances on DSP brings this solution to the table.

To conclude, the signal used in the MORFEUS network is represented in figure 2.19. Despite the fact that the MORFEUS signal uses virtual carriers to aid in the detection of each OFDM band, the SSB MB-OFDM signal represented in figure 2.19 also includes the optical carrier. The optical carrier may be needed to feed the electro-optic modulator of each node and to ensure relaxed constraints caused by laser phase noise and laser wavelength drift.

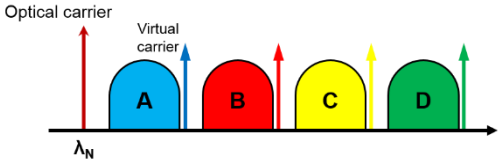

Figure 2.19 - SSB MB-OFDM optical signal with virtual carriers used in MORFEUS network.

2.3.4 Multiband-OFDM signal parameters

As it was shown in figure 2.19, the MB-OFDM signal used in the MORFEUS project is composed by several bands. The central frequency of each band is related with the central frequency of the other bands through the equation (considering that all OFDM bands have the same bandwidth):

$$f_{c,n} = f_{c,n-1} + \Delta f = f_{c,n-1} + BG + B_w, \qquad n \in \{2,...,N_B\} \tag{2.29}$$

where $f_{c,n}$ represents the central frequency of the n-th band, N_B is the total number of bands, BG is the gap between consecutive bands, B_w is the bandwidth of the OFDM band and Δf is the band spacing (which in this system is 3.125 GHz). Figure 2.20 represents the parameters of equation 2.29.

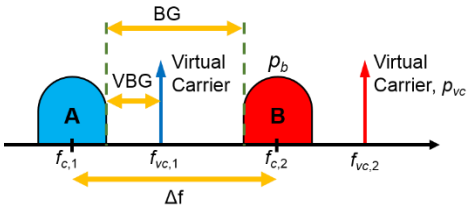

Figure 2.20 - Illustration of the parameters that describe the OFDM bands of a MB-OFDM signal employing virtual carriers.

Figure 2.20, shows also the virtual carrier of each OFDM band. The frequency of each virtual carrier depends on the band gap between the OFDM band and the frequency of the virtual carrier. This band gap is the virtual band gap (VBG) and the frequency of the virtual carrier is given by:

$$f_{vc,n} = f_{c,n} + \frac{B_w}{2} + VBG, \tag{2.30}$$

where $f_{vc,n}$ is the virtual carrier frequency of the n-th band. Both OFDM band and virtual carrier are characterized by a power, in which p_b is the power of the OFDM band and p_{vc} is the power of the virtual carrier. These two powers are related through the virtual carrier-to-band power ratio (VBPR) given by

$$vbpr = \frac{p_{vc}}{p_b}. \tag{2.31}$$

The following graphs, represented in figures 2.21 and 2.22, were obtained to describe the impact of the SSBI on the value defined for the VBG as well as the impact of the DP-MZM modulation index on the system performance. The parameters of the system used to obtain these graphs were: 128 subcarriers, 10 OFDM symbols (in which 8 are training symbols) and one OFDM band with central frequency of 2 GHz. The frequency of the VC frequency varied according to the VBG value tested. The bandwidth of the OFDM band was calculated using equation 2.15, considering an OFDM symbol period of 312.5 ns and a guard interval of 70.1 ns, which results in 530.33 MHz. The modulation used was 4-QAM, the DAC was used in sample and hold mode and the value defined for the VBPR was 6 dB.

In section 2.3.3, it is explained that the SSBI distortion, when using virtual carriers, lies between the OFDM band and the virtual carrier. Therefore, unless DSP algorithms are used to mitigate the SSBI term, the MB-OFDM system only works properly if the VBG is greater than the bandwidth of the OFDM band. This can be verified through figure 2.21, where the EVM (explained in appendix A.5) is represented as a function of the VBG, for four different modulation indexes, *m,* from equation 2.24.

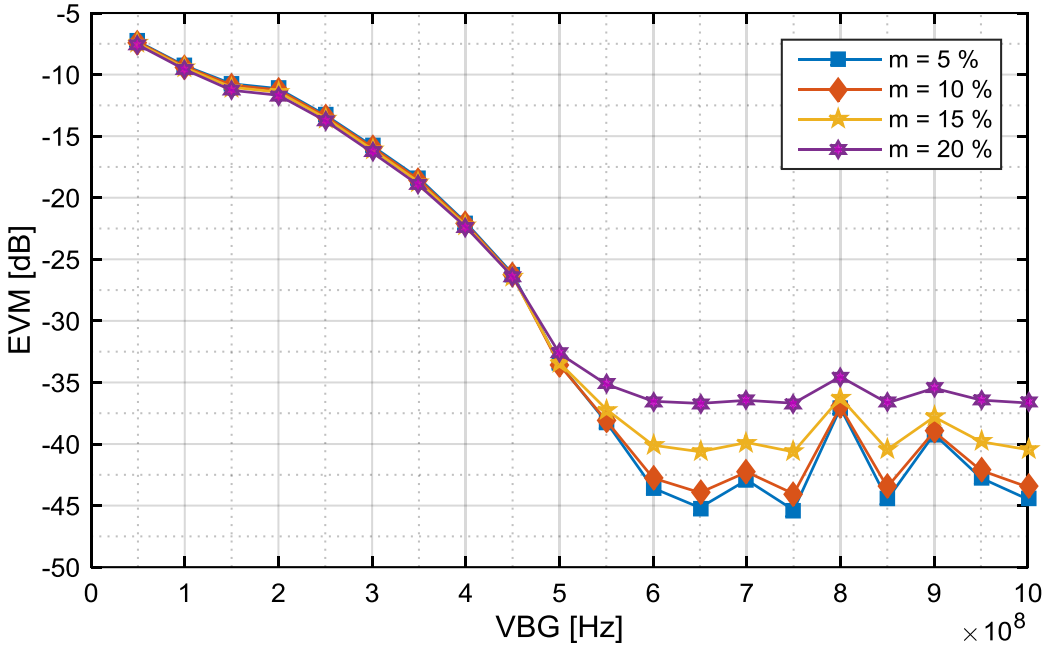

Figure 2.21 - EVM in function of the VBG, for four different modulation indexes.

It is possible to observe that, when the VBG starts to exceed the OFDM bandwidth, around 550 MHz, the values of EVM tend to be very low. Also, when the modulation index is lower, the EVM is lower as well. To illustrate this last conclusion, it is represented in figure 2.22 the EVM as a function of the modulation index. In this case, the VBG (550 MHz) was defined to be higher than the OFDM band bandwidth (530.33 MHz), in order to show how the EVM varies with the increase of the modulation index.

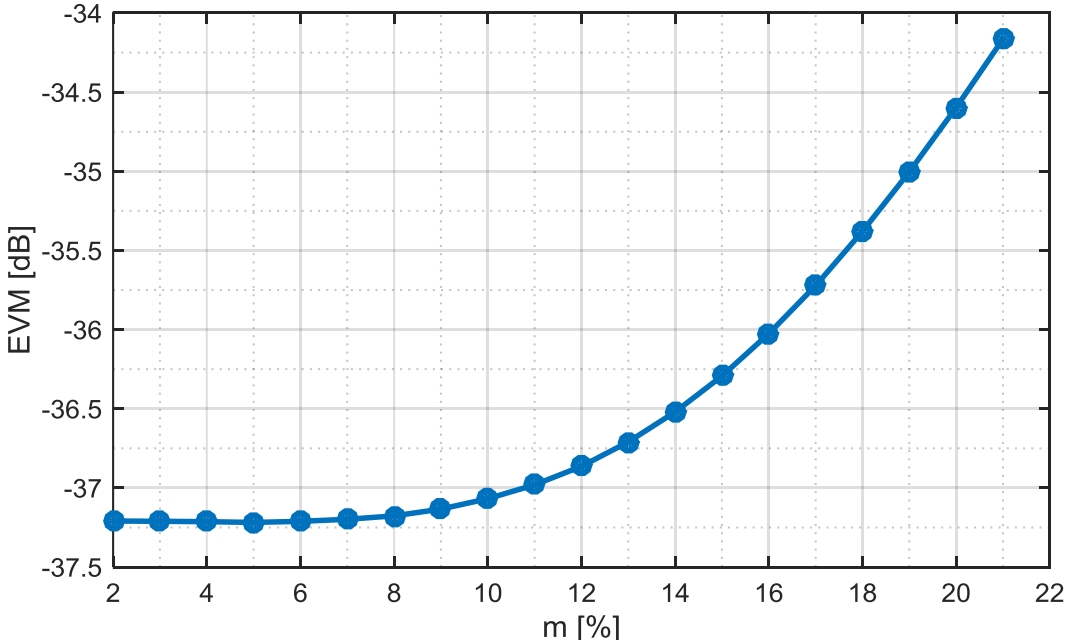

Figure 2.22 - EVM as a function of the modulation index, for a VBG of 550 MHz.

With figure 2.22, it is possible to observe the degradation suffered by the EVM when the nonlinearities of the DP-MZM start to interfere with the OFDM signal.

The signal used on this work is, as mention before, an MB-OFDM signal, so its bitrate is composed by the bitrate of its bands. This bitrate, $R_{b,MB\text{-}OFDM}$, is given by

$$R_{b,MB-OFDM} = \sum_{n=1}^{N_B} R_{b,n} \tag{2.32}$$

where $R_{b,n}$ is the bitrate of the n-th OFDM band, which can be calculated through equation 2.14. Considering that all OFDM band parameters are the same, then the MB-OFDM signal bitrate can be simplified to

$$R_{b,MB-OFDM} = N_B R_b \tag{2.33}$$

where R_b is the bitrate of a OFDM band.

Additionally, another parameter that describes the MB-OFDM signal used is its bandwidth. The MB-OFDM signal bandwidth is defined by:

$$B_{w,MB-OFDM} = \sum_{n=1}^{N_B} B_{w,n} + \sum_{i=1}^{(N_B-1)} BG \tag{2.34}$$

where $B_{w,n}$ is the bandwidth of each OFDM band, which can be calculated through equation 2.15.

As stated before, the bitrate and bandwidth of a single OFDM band can be calculated through equation 2.14 and 2.15. However, on the upcoming analysis, it is considered a simplified yet accurate approximation for the bitrate and bandwidth. This equation is based on equations 2.13 and 2.15. From equation 2.15, considering that the guard interval is much smaller than the OFDM signal period then $\left(T_s - \Delta_G\right) \approx 1$; also, since the value of the number of subcarriers N_{sc} (128 subcarriers) is much higher than 1, therefore the nominator from equation 2.15 is $2 + N_{sc} - 1 = N_{sc} + 1 \approx N_{sc}$. With these simplifications, the OFDM signal bandwidth can be given by:

$$B_w = \frac{N_{sc}}{T_s} \tag{2.35}$$

With equation 2.35 and 2.13, the bitrate can be calculated using the signal bandwidth, given by:

$$R_b = B_w \times \log_2 M; \tag{2.36}$$

2.3.5 Multiband-OFDM system parameters

The system described in this work is designed for a bitrate of 100 Gbit/s and 16-QAM modulation. The target BER is 10^{-3}, which is can be lowered to 10^{-15} thanks to the use of FEC with overhead of 12 % [59, 60]. Therefore, the target bitrate increases to 100 * 1.12 = 112 Gbit/s.

Since this MB-OFDM system is designed to have a channel spacing of 50 GHz with only 75% being used and the OFDM bands are spaced by a Δf of 3.125 GHz, the number of OFDM bands that can be used are 12.

Therefore with 112 Gbit/s target bitrate and 12 OFDM bands, the bitrate per OFDM band becomes 9.33 Gbit/s. Using equation 2.35 this results in an OFDM bandwidth of 2.33 GHz and an OFDM signal period of 54.86 ns. These parameters will be used during the assessment of the minimum required optical signal-to-noise ratio (OSNR) in chapter 4.

2.3.6 MORFEUS node

To ensure a good transportation through the metro ring, the nodes present in the MORFEUS network must be able to insert, extract and pass-through the bands from the MORFEUS signal shown before. In figure 2.23, it is represented a schematic of a MORFEUS node. When a WDM MB-OFDM signal enters the MORFEUS node, the signal is demultiplexed in the ROADM. Then, the output of the demultiplexer is connect to the MORFEUS insertion blocks (MIBs) and MORFEUS extraction blocks (MEBs), through optical switches. The currently used ROADMs contain the multiplexers, demultiplexers and the optical switches integrated in a single device [50].

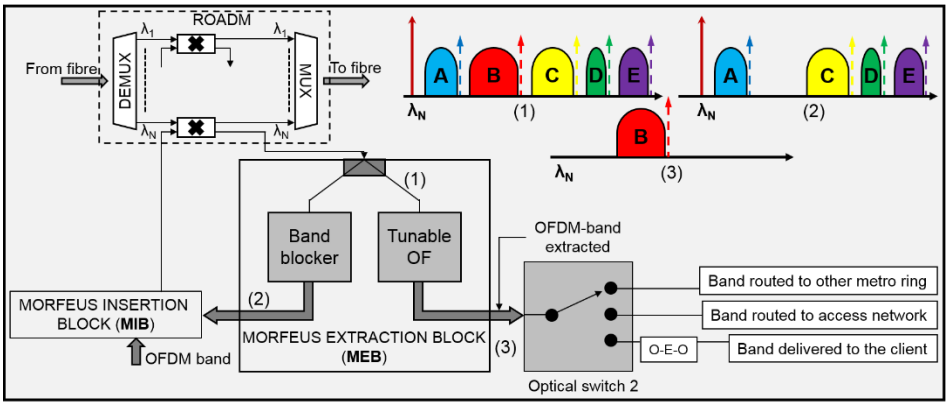

Figure 2.23 - Schematic diagram of the MORFEUS node comprising the MORFEUS insertion block (MIB) and the MORFEUS extraction block (MEB) [5].

In figure 2.23, the optical switch 1, can be in two positions. If the optical switch is in cross position, then the MB-OFDM signal enters the MEB. In the MEB, the MB-OFDM signal is processed by two different blocks. When the signal is processed in the Tunable OF (optical filter), the assigned band to that node is extracted and enters the optical switch 2. In this switch, the band can be routed to other metro ring; routed to an access network or delivered to the client in the electrical domain. When the signal is processed by the band blocker, this block removes the band assigned to the node, leaving a gap to be filled by the MIB. In the MIB, this gap can be filled by a band that is originated from another metro ring or access network, in the optical domain, or by a new band that has been created from the electrical domain. If the optical switch 1 is in bar position, the MB-OFDM signal passes through, without performing add and drop actions. The different wavelengths are then multiplexed to form the WDM MB-OFDM signal, in order to be transmitted along the optical fibre to the next node.

Figure 2.23 represents also three cases of the spectral occupancy of the MB-OFDM signal, through three points of the MORFEUS node. The first case represents the MB-OFDM signal when it enters the MEB. The second case represents the signal after removing the assigned band to the node,

resulting in a MB-OFDM signal with a free band slot. The third case represents the band that was dropped by the tunable optical filter and is prepared to be routed.

2.3.7 Optical fibre

The transmission medium considered in this work is the optical fibre. Optical fibres can be categorized into two main groups, single-mode fibres and multi-mode fibres, depending on the number of propagation modes supported. The type of optical fibre used in metro networks is the standard single-mode fibre (SSMF).

Although an optical fibre is a non-linear transmission medium, the optical fibre non-linear effects, like for example self-phase modulation (SPM), four-wave mixing (FWM), cross-phase modulation (XPM) [35], are not considered in this work. In this work, the optical fibre is considered as a linear transmission medium. There are two optical fibre characteristics that need to be taken into account. The first one is the fibre dispersion, which is caused by different signal components travelling at different velocities in the optical fibre, causing them to arrive at the receiver at different time stamps. This causes temporal distortion on the transmitted signal and leads to ISI. The second one is the fibre losses, responsible for the signal attenuation.

In this work, the model used to describe the impact of the optical fibre effects on the performance of the system is based on the equivalent baseband transfer function of the SSMF [35] and given by

$$H_f\left(\Delta\omega\right) = e^{\frac{-\alpha L_f}{2}} e^{-j\beta(\Delta\omega)L_f} \tag{2.37}$$

where the first term describes the fibre losses and the second term describes the fibre dispersion.

In equation 2.37, α represents the fibre attenuation coefficient in Np/m, L_f the length of the optical fibre, β the propagation constant in rad/m and $\Delta\omega$ the equivalent baseband angular frequency, which represents the deviation from the optical frequency v_0 in Hz.

The fibre attenuation α depends on the optical frequency. However, in the C-band (frequency band from 1530 to 1565 nm), its value practically does not vary and it is approximately equal to 0.2 dB/km [57].

The propagation constant β also depends on the optical frequency. Like α, its value cannot be calculated, but since the propagation constant is responsible for pulse broadening [58], an approximation is needed in order to evaluate its impact on the system. Based on the Taylor series, an approximation is used when the signals' bandwidth is much lower than v_0. This approximation is given by

$$\beta \approx \beta_0 + \beta_1\left(\Delta\omega\right) + \frac{\beta_2}{2}\left(\Delta\omega\right)^2 + \frac{\beta_3}{6}\left(\Delta\omega\right)^3. \tag{2.38}$$

In equation 2.38, β_0 represents the propagation constant at the carrier frequency and $\beta_1\left(\Delta\omega\right)$ the propagation delay. These two terms are not accounted in this work since they do not add dispersion to the signal. Therefore, only the two latter terms are considered, where β_2 represents the group velocity dispersion (GVD) and β_3 the second order GVD. Their expressions can be given by

$$\beta_2 = -\frac{\lambda_0^2 D_{\lambda_0}}{2\pi c}$$
$$\beta_3 = \left(\frac{\lambda_0^2}{2\pi c}\right)^2 S_{\lambda_0} + \frac{\lambda_0^3 D_{\lambda_0}}{2\pi^2 c^2} \quad (2.39)$$

From both equations 2.38 and 2.39, c is the speed of light in the vacuum, λ_0 the wavelength of the optical frequency (λ_0=c/v_0), $D_{\lambda 0}$ the dispersion parameter of the optical fibre for the λ_0 and $S_{\lambda 0}$ the slope parameter for λ_0. In this work v_0 = 193.1THz, λ_0 = 1552.52 nm, the speed of light, c, 299792458 ms^{-1}, $D_{\lambda 0}$ = 17ps/nm/km and $S_{\lambda 0}$ = 70 $fs/nm^2/km$.

So, using equation (2.38) on the initial equation from the model of the optical fibre, this mathematical model can be rewritten as

$$H_f(\Delta\omega) = e^{\frac{-\alpha L_f}{2}} e^{-j\left(\frac{\beta_2}{2}(\Delta\omega)^2 + \frac{\beta_3}{6}(\Delta\omega)^3\right)L_f} \quad (2.40)$$

After deducing the equation for the SSMF optical fibre model, it was possible to determine its impact on the MB-OFDM system. This impact was evaluated using four lengths of optical fibre. As indicated before, the dispersive effect of the fibre leads to ISI and ICI. According to equation 2.10, to neglect this effect, the time delay spread needs to be inferior to the guard band interval. The time delay spread can be given by

$$t_d = D_{\lambda_0} L_f \Delta\lambda_s \quad (2.41)$$

where $\Delta\lambda_s$ represents the spectral width of the optical signal. Since the guard band interval is added to each band, the spectral width can be given by

$$\Delta\lambda_s = \frac{\lambda_0^2}{c} B_{OFDM}. \quad (2.42)$$

Since four lengths of optical fibre were used on the following evaluations and considering that the CP is equal to the guard band interval, four values of CP were considered as well. Using equations 2.41 and 2.42, for 100 km the CP is 31.88 ps, for 200 km the CP is 63.76 ps, for 300 km the CP is 95.64 ps and for 400 km the CP is 127.52 ps.

2.4 Conclusions

In this chapter, the general principles of OFDM were presented along with the blocks that integrate the OFDM system architecture, which is used to generate an OFDM signal. Lastly, it was given a brief description of the problems that OFDM signals suffer from, like the PAPR, frequency offset and phase noise.

Moreover, the DDO-OFDM system was described, where the main performance limitation, the SSBI, was introduced. Then the MB-OFDM system, the MB-OFDM signal and the MB-OFDM node were introduced and described.

As it was said in section 2.3.3, in order to mitigate the SSBI term and at the same time maintain an high spectral efficiency, VBG needs to be minimum, smaller than the OFDM band. This can only be

achieved through the implementation of DSP algorithms. So it can be concluded that the implementation of algorithms based on memory polynomials is needed. These algorithms will be introduced in chapter 3.

Chapter 3 - Memory polynomials theory

In this chapter, the memory polynomial theory is introduced and described. The best structure of the memory polynomial to mitigate the SSBI is determined. The band selector used in the MB-OFDM system of this dissertation is presented and its optimum parameters are defined.

3.1 Mathematical definition of the memory polynomial

In section 1.1.5, the theme of the memory polynomials was introduced. The use of these memory polynomials is intended to evaluate their capability to mitigate the main non-linearity present in the DD systems, the SSBI. To accomplish this and as it was referred in section 1.1.5, to mitigate the distortion present in the system *S* (system containing the transmitter and the receiver) the memory polynomials are used to implement an inverse system S^{-1}, which is then going to be used to mitigate the SSBI and at the same time other nonlinearities that appear alongside transmission. To define a memory polynomial that can represent an inverse of the system *S*, the system *S* needs to be described by the Volterra series [18]. A discrete version of the Volterra series that describes a nonlinear causal system *S* with finite memory can be given by [22]

$$y[n]=\sum_{p=1}^{P}\sum_{q_1=0}^{a_p}\cdots\sum_{q_p=0}^{a_p}h_p\left(q_1,q_2,\ldots,q_p\right)\prod_{m=1}^{p}x\left[n-q_m\right] \tag{3.1}$$

where $x[n-q_m]$ represents the input signal $x[n]$ delayed by q_m samples, $y[n]$ represents the samples of the output signal, $h_p(q_1,q_2,\ldots,q_p)$ is the p-th order discrete Volterra kernel (DVK) of the system *S*, *P* represents the highest nonlinear order of system *S* and a_p represents the maximum sample delay from the p-th order DVK. The Volterra discrete series given in equation 3.1 is a summation weighted by the values of $h_p(q_1,q_2,\ldots,q_p)$. These values can also be expressed in a form of a memory polynomial (MP). The same happens to the inverse system S^{-1}, which means that an inverse system of *S* can be expressed through a MP. Considering that the system is time-invariant many coefficients become redundant and can be discarded. According to [61], a simplified model of the memory polynomial is given by

$$\begin{aligned}y(n)=&\sum_{k_a=1}^{K_a}\sum_{q_a=0}^{Q_a}w_a\cdot x^{k_a}\left(n-q_a\right)+\sum_{k_b=1}^{K_b}\sum_{q_b=0}^{Q_b}\sum_{m_b=1}^{M_b}w_b\cdot x\left(n-q_b\right)\cdot x^{k_b}\left(n-q_b-m_b\right)\\&+\sum_{k_c=1}^{K_c}\sum_{q_c=0}^{Q_c}\sum_{m_c=1}^{M_c}w_b\cdot x\left(n-q_c\right)\cdot x^{k_c}\left(n-q_c+m_c\right)\end{aligned} \tag{3.2}$$

where w_a, w_b and w_c represent the Volterra kernel coefficients $h_p(q_1,q_2,\ldots,q_p)$, *x(n)* the input signal and K_a, Q_a, K_b, Q_b, M_b, K_c, Q_c and M_c the parameters of the MP, more specifically, K_a, K_b and K_c indicate the order of the MP and the rest indicates the delays applied to the input signal x. The number of coefficients, N_C, that compose the memory polynomial represented in (3.2) can be calculated through expression (3.3)

$$N_C=K_a\cdot\left(Q_a+1\right)+K_b\cdot\left(Q_b+1\right)\cdot M_b+K_c\cdot\left(Q_c+1\right)\cdot M_c \tag{3.3}$$

in which $K_a \cdot (Q_a + 1)$ represent the coefficients that belong to the signal where the delays applied are the same, equal to q_a; $K_b \cdot (Q_b + 1) \cdot M_b$ the coefficients that represent the lagging terms of signal x in which the delays are of different durations, being the first delay q_b and the second q_b+m_b and $K_c \cdot (Q_c + 1) \cdot M_c$ give the coefficients that represent the leading terms of signal x. In this case the delays are also different, but although the first one is equivalent to the previous case, q_c, the second delay is q_c-m_c. The delays represent the memory of the MP. This means that when a MP has a high delay, it has an high memory, leading to a MP that can compensate more dispersive effects, with the cost of computer simulation.

The coefficients **w**, (*w* is composed by the coefficients w_a, w_b and w_c), are obtained by estimation. This estimation is performed in three steps: (1) capturing N_S samples from the input and output signals, *x* and *y*, respectively; (2) creating the matrix **V** from the sampled signal *y*, and finally, (3) calculating the vector **w** (which contains the coefficients *w*) from matrix **V** and the sampled input signal **x**, through expression (3.4) [22]

$$\begin{cases} \mathbf{w} = \left(\mathbf{V}^{\mathrm{H}}\mathbf{V}\right)^{-1}\mathbf{V}^{\mathrm{H}} \cdot \mathbf{x} = \mathbf{V}^{-1} \cdot \mathbf{x} \\ \mathbf{x} = \left[x[1], x[2], \ldots, x[N_S]\right]^T \end{cases}. \tag{3.4}$$

where $(.)^T$ denotes the transpose operation and $(.)^H$ the complex conjugate transpose operation. The matrix **V**, referred in step (3), is a matrix with N_S rows and N_C columns. To facilitate the understanding on how matrix **V** is composed, it can be considered that matrix **V** has three inner matrixes, one for each component of the memory polynomial presented in (3.2),

$$\mathbf{V} = \begin{bmatrix} \mathbf{V}_A & \mathbf{V}_B & \mathbf{V}_C \end{bmatrix}. \tag{3.5}$$

The matrix **V** can then be calculated through expression (3.6)

$$\mathbf{V} = \begin{bmatrix} y^{k_a}[1-q_a] & y[1-q_b]y^{k_b}[1-q_b-m_b] & y[1-q_c]y^{k_c}[1-q_c+m_c] \\ \vdots & \vdots & \vdots \\ \vdots & \vdots & \vdots \\ \underbrace{y^{k_a}[N_S-q_a]}_{\mathbf{V}_A} & \underbrace{y[N_S-q_b]y^{k_b}[N_S-q_b-m_b]}_{\mathbf{V}_B} & \underbrace{y[N_S-q_c]y^{k_c}[N_S-q_c+m_c]}_{\mathbf{V}_C} \end{bmatrix}. \tag{3.6}$$

3.2 Memory polynomial implementation

The memory polynomial presented in expression (3.2) is implemented in the digital signal processor (DSP). The DSP is located at the receiver, after the PIN photodetector, as it is represented in figure 3.1.

Since the DSP is located at the receiver, this MP implementation is called digital post-distortion. The SSBI mitigation process using the MP from expression (3.2) is:

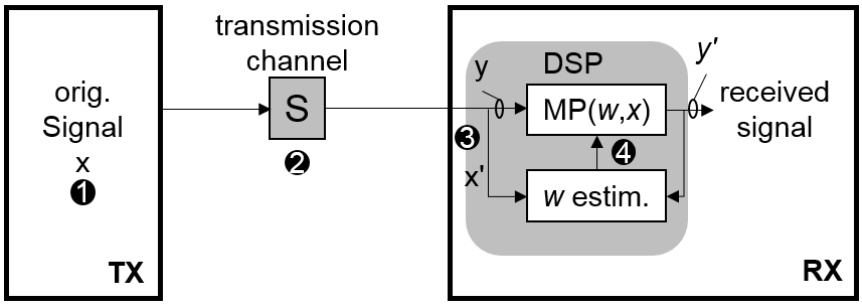

Figure 3.1 - Location of the DSP on the MB-OFDM system.

1 – The OFDM signal is created at the transmitter and it is composed by the training symbols and information symbols.

2 – The OFDM signal enters the optical modulator (DP-MZM in this work) and its output enters the transmission channel (optical fibre). At the receiver, it passes through the band selector (2nd order super Gaussian filter) and is photodetected in the PIN, passing from the optical to the electrical domain.

3 – The received electrical signal then enters the DSP where the transmitted signal x is reconstructed using the training symbols. Using the reconstructed signal x' and the samples from the received signal corresponding to the training symbols, the coefficients of the MP are estimated.

4 – With the coefficients and the complete received signal, the signal without the effect of the SSBI is created and used for processing.

3.3 Evaluation of the best structure for the memory polynomial

To determine the best structures of the MP that were able to mitigate the SSBI, a test that returned approximately 204000 results was executed. The system considered in this test was noise free and its parameters are represented in table 3.1. The first half of the signal x was used to estimate the coefficients because it corresponds to the samples of the training symbols, which are known.

Table 3.1 - System parameters used in the tests executed.

Parameter	Value	Parameter	Value
Number of subcarriers	128	Central frequency of the 1st band [GHz]	2
Number of OFDM symbols	200	OFDM band bandwidth [GHz]	2.5
Number of OFDM training symbols	100	VBG [MHz]	90
Number of samples per chip	32	Modulation order	16QAM
Sampling mode	S&H	VBPR [dB]	7
Number of samples N_s	528000	Average power at the output of the DP-MZM [dBm]	0
Number of OFDM bands	1	Modulation index [%]	10
Binary rate of each band [Gbit/s]	10	Bias point of inner MZM 1	MBP
OFDM symbol period [ns]	51.2	Bias point of inner MZM 2	MBP
Cyclic prefix [ns]	12.8	Bias point of DP-MZM	QBP

The cases that integrated this test were chosen to determine if the three components of the MP of (3.2) were necessary. Therefore, the following six cases were considered:

i. represented in expression 3.7, the first summation from expression (3.2) without any delay Q_a. This test was meant to evaluate if the memory polynomial was able to correct the nonlinearities without memory;

$$y(n) = \sum_{k_a=1}^{K_a} w_{ia} \cdot x^{k_a}(n) \tag{3.7}$$

ii. represented in expression 3.8, the first summation from expression (3.2), but this time with memory ($Q_a \neq 0$);

$$y(n) = \sum_{k_a=1}^{K_a} \sum_{q_a=0}^{Q_a} w_{ia} \cdot x^{k_a}(n-q_a) \tag{3.8}$$

iii. represented in expression 3.9, the third summation from expression (3.2), which was intended to see if the terms of the same order of the transmitted signal are important to the MP;

$$y(n) = \sum_{k_c=1}^{K_c} \sum_{q_c=0}^{Q_c} \sum_{m_c=1}^{M_c} w_{ib} \cdot x(n-q_c) \cdot x^{k_c}(n-q_c+m_c) \tag{3.9}$$

iv. represented in expression 3.10, the first and the second summation from expression (3.2), which will from now on be referred as the past MP. In this case, the intention was to evaluate how the MP would behave with just negative delays, in others words, how the memory polynomial would behave with just the lagging terms of the signal x;

$$y(n) = \sum_{k_a=1}^{K_a} \sum_{q_a=0}^{Q_a} w_{ia} \cdot x^{k_a}(n-q_a) + \sum_{k_b=1}^{K_b} \sum_{q_b=0}^{Q_b} \sum_{m_b=1}^{M_b} w_{ib} \cdot x(n-q_b) \cdot x^{k_b}(n-q_b-m_b) \tag{3.10}$$

v. represented in expression 3.11, the first and the third summation from expression (3.2), which will from now on be referred as the future MP. This case was intended to see how the memory polynomial would behave with just the leading terms of the signal x. In this case, although the first summation does not have leading terms, it is necessary to represent the first order of the MP which is the signal x;

$$y(n) = \sum_{k_a=1}^{K_a} \sum_{q_a=0}^{Q_a} w_{ia} \cdot x^{k_a}(n-q_a) + \sum_{k_c=1}^{K_c} \sum_{q_c=0}^{Q_c} \sum_{m_c=1}^{M_c} w_{ib} \cdot x(n-q_c) \cdot x^{k_c}(n-q_c+m_c) \tag{3.11}$$

vi. finally, the first, second and third summation from expression (3.2), which will from now on be referred as the complete MP. This case investigates the performance of the complete MP.

Having chosen the cases that were going to be assessed, it had to be chosen the structures of the MP that were to be tested. It was decided that the order of the MP should not be higher than 5 and the delays should not be more than 5. Therefore, the complete memory polynomial had the structure

$$\begin{aligned} y(n) = & \sum_{k_a=1}^{4} \sum_{q_a=0}^{4} w_a \cdot x^{k_a}(n-q_a) + \sum_{k_b=1}^{4} \sum_{q_b=0}^{4} \sum_{m_b=1}^{5} w_b \cdot x(n-q_b) \cdot x^{k_b}(n-q_b-m_b) \\ & + \sum_{k_c=1}^{4} \sum_{q_c=0}^{4} \sum_{m_c=1}^{5} w_c \cdot x(n-q_c) \cdot x^{k_c}(n-q_c+m_c). \end{aligned} \tag{3.12}$$

Before the test was executed, the starting EVM of the system without any mitigation for the SSBI was -10.5 dB. The constellation at the receiver with no SSBI mitigation is represented in figure 3.2 in blue and with ideal SSBI mitigation in orange.

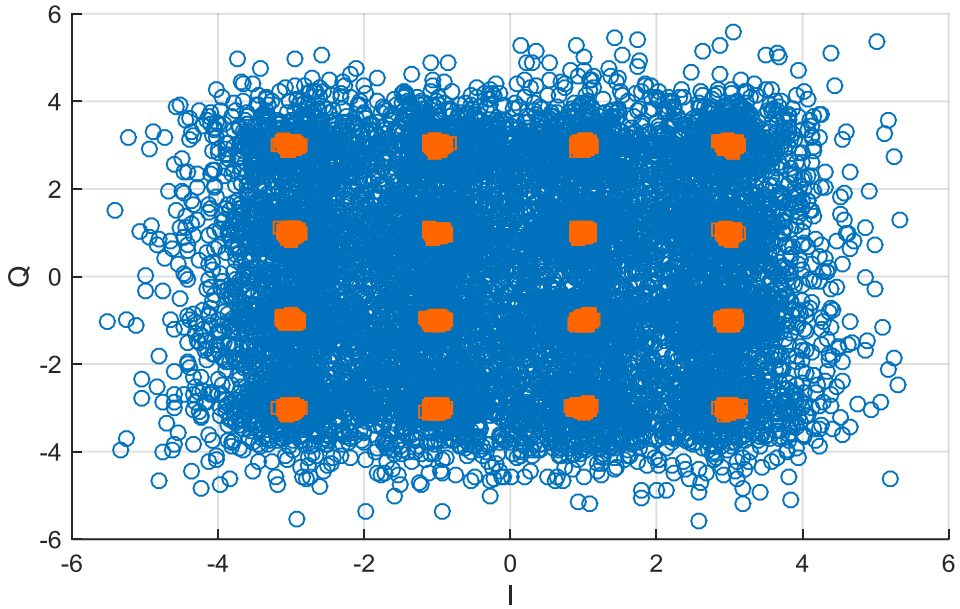

Figure 3.2 - Constellation at the receiver when no SSBI mitigation is used.

3.3.1 First analysis: Structures with EVM lower than the initial

After obtaining the results, it was executed a preliminary analysis, in which it was concluded that the first three cases presented above (expression 3.7, 3.8 and 3.9) were not important to consider because the EVM values obtained were the same as the beginning or worse. Therefore these three cases were discarded. The latter three cases, after this preliminary analysis, presented improvements to the system performance and so, they were kept for further analysis.

3.3.2 Second analysis: Structures that achieved the lowest EVM value

The second analysis made to the latter three cases (past MP, future MP and complete MP) was intended to find the structures that were able to achieve the better system performance, without taking into account the number of coefficients required. It was always considered at least one structure of each case (the past, future and complete MP) in order to compare and evaluate if the three components of the MP shown in expression (3.2) were important or if one of them could be discarded. The structures that were chosen in this second analysis are presented in table 3.2.

In table 3.2, there are represented the memory polynomial structures that presented the best performance improvement. It is also represented the number of coefficients that each structure requires to achieve that performance improvement. Although it is said that the number of coefficients was not a decision factor in this second analysis, since there were several cases with similar EVM values and different coefficients used, then it were considered the structures that used the less coefficients (marked in grey).

Table 3.2 - First analysis results: best structures based only on the performance achieved.

K_a	Q_a	K_b	Q_b	M_b	K_c	Q_c	M_c	EVM [dB]	N_C
Past MP structure									
4	4	4	4	5	0	0	0	-16.69	120
Future MP structure									
2	3	0	0	0	4	4	5	-16.98	108
2	4	0	0	0	4	4	5	-17.01	110
3	4	0	0	0	4	4	5	-17.03	115
4	4	0	0	0	4	4	5	-17.03	120
Complete MP structure									
1	2	4	4	5	4	2	5	-17.07	163
1	4	4	4	5	4	2	4	-17.01	153
3	4	4	4	5	4	2	4	-17.02	163
4	4	4	4	5	4	2	5	-17.00	160
4	4	4	4	5	4	1	5	-16.99	160

After choosing the best structures for each case using only the performance as a criterion, it was conducted a third analysis in which the number of coefficients was taken into account.

3.3.3 Third analysis: Structures with the best relation between number of coefficients used and EVM achieved

In this third analysis, the number of coefficients required by each MP structure was taken into account when deciding which of the structures was considered to be the better relation between performance achieved (EVM value) and complexity required (coefficients). To perform this analysis, it was considered a starting structure for the past and future MP (marked in grey in table 3.2) and then each parameter (K_a, Q_a, K_b, Q_b, M_b, K_c, Q_c and M_c) was altered to see how the EVM value and coefficient number would vary. The approach used to perform the third analysis on the complete MP was different and shall be explained further below.

- Past MP

In this third analysis, the first case to analyse was the past MP, represented in table 3.3. First, the order K_a was varied and it was concluded that for a lower value of K_a (two and three) the EVM is similar to the EVM shown in table 3.2:

Table 3.3 - Variation of the order Ka.

K_a	Q_a	K_b	Q_b	M_b	K_c	Q_c	M_c	EVM [dB]	N_C
2	4	4	4	5	0	0	0	-16.67	110
3	4	4	4	5	0	0	0	-16.67	115

Then, the value of order K_b was changed and the conclusion was that the EVM was worse when the value of K_b is lower, which meant that the order of the memory polynomial must be five. When the value of the delays Q_a, Q_b and M_b were changed, the EVM increases, which meant that the initial values were the important ones.

Therefore, the best structure of the past memory polynomial is represented in table 3.4:

Table 3.4 - Best structure of the past MP.

K_a	Q_a	K_b	Q_b	M_b	K_c	Q_c	M_c	EVM [dB]	N_C
2	4	4	4	5	0	0	0	-16.67	110

- Future MP

The second case to be analysed was the future memory polynomial, marked in grey in table 3.2. In this case the variation of the value K_c was tested first and the only value of K_c that achieved a good EVM was 4, meaning that the memory polynomial had to be of 5th order. Then, when changing the values of the delays Q_c and M_c, the EVM was worse, which meant that these delays were correct. When the values of order K_a and the delay Q_a were changed the possibilities were many. Taking into account the number of coefficients used and the performance achieved, the possibilities were reduced to five cases listed in table 3.5.

Table 3.5 – Structures of the future MP that achieved the best performance when varying K_a and Q_a.

K_a	Q_a	K_b	Q_b	M_b	K_c	Q_c	M_c	EVM [dB]	N_C
1	1	0	0	0	4	4	5	-16.65	102
4	1	0	0	0	4	4	5	-16.82	108
1	2	0	0	0	4	4	5	-16.72	103
2	2	0	0	0	4	4	5	-16.96	106
2	3	0	0	0	4	4	5	-16.98	108

After analysing the possibilities presented in table 3.5, it was concluded that the best relation between low number coefficients used and EVM achieved, was the case selected in grey.

- Complete MP

Finally, as stated before, the approach used to perform the third analysis was different when it was applied to the results of the complete MP. This occurred because, since the complete MP had 200000 different possibilities, it was impossible to analyse by altering the MP parameters one by one. Therefore it was used a different approach. The 200000 possibilities were divided into groups. These groups contained only structures with an achieved EVM lower than -16.5 dB. The parameter used to divide the possible structures into groups was the number of coefficients used, for example, the first group was for structures that used between 70 and 79 coefficients, and so on.

After dividing by groups it was concluded that the EVM of MPs with a number of coefficients between 70 and 79 were around -16.5 dB. When the coefficients were between 80 and 89, there was a

case that achieved a value of EVM inferior to -16.5 dB and was the lowest compared to the others in that same group. This case which is represented in table 3.6.

Table 3.6 - Best structure of the complete MP.

K_a	Q_a	K_b	Q_b	M_b	K_c	Q_c	M_c	EVM [dB]	N_C
3	4	4	1	5	4	1	4	-16.76	87

As the analysis continued group by group, there was not any other structure that could achieve the EVM represented above with less coefficients. Therefore this is considered to be the best structure for the complete MP, which presents a good ratio between the number of coefficients used and the EVM achieved. When compared with the structure selected in the second analysis, it can be concluded that this new structure uses less coefficients (less 66). Although the EVM value is a little higher (around 0.2 dB) with the structure from table 3.6, the gain in computer simulation is worth the degradation in performance.

With the third analysis concluded the best MP structure chosen for each case is represented in table 3.7.

Table 3.7 - Best structures for the past, future and complete MP.

K_a	Q_a	K_b	Q_b	M_b	K_c	Q_c	M_c	EVM [dB]	N_C
Past MP structure									
2	4	4	4	5	0	0	0	-16.70	110
Future MP structure									
2	2	0	0	0	4	4	5	-16.96	106
Complete MP structure									
3	4	4	1	5	4	1	4	-16.76	87

The spectrum at the DSP output, when the complete MP structure from table 3.7 is used to mitigate the SSBI, is represented in figure 3.3. The spectrum for the past and future MP is similar to the spectrum of the complete MP.

In figure 3.3, it is marked in white the OFDM band. To demonstrate the correction made by the MP it is represented in figure 3.4 (left) and 3.4 (right) the spectrum of the input of the DSP and the output respectively. The figures have been zoomed in the area corresponding to the SSBI to evidence the mitigation done on the output of the DSP.

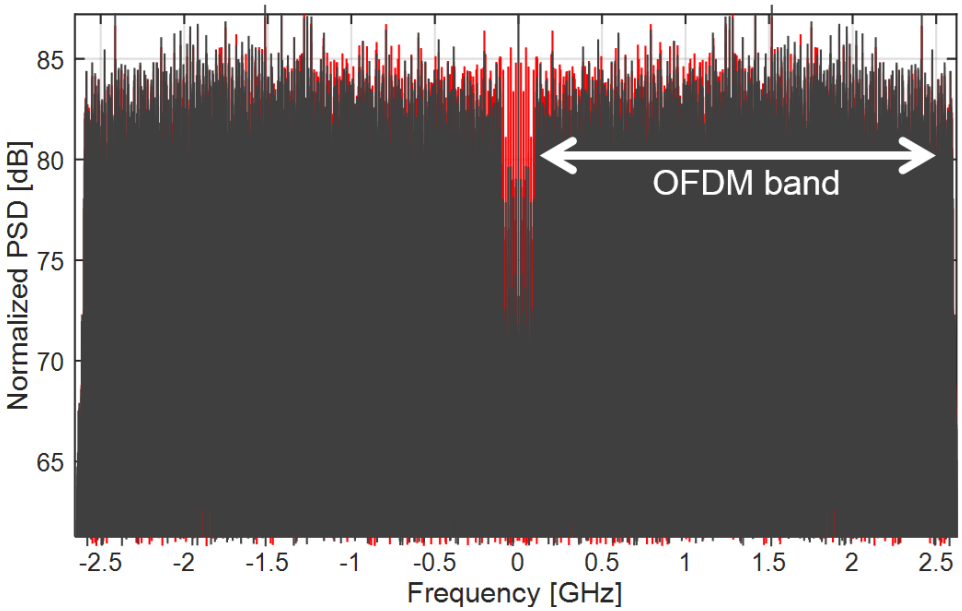

Figure 3.3 - Spectrum at the DSP output. The spectrum on the back (red) is at the DSP input. On top (grey) is the spectrum at the DSP output.

When comparing the two figures it is possible to see the reduced SSBI distortion on the left figure, the output of the DSP.

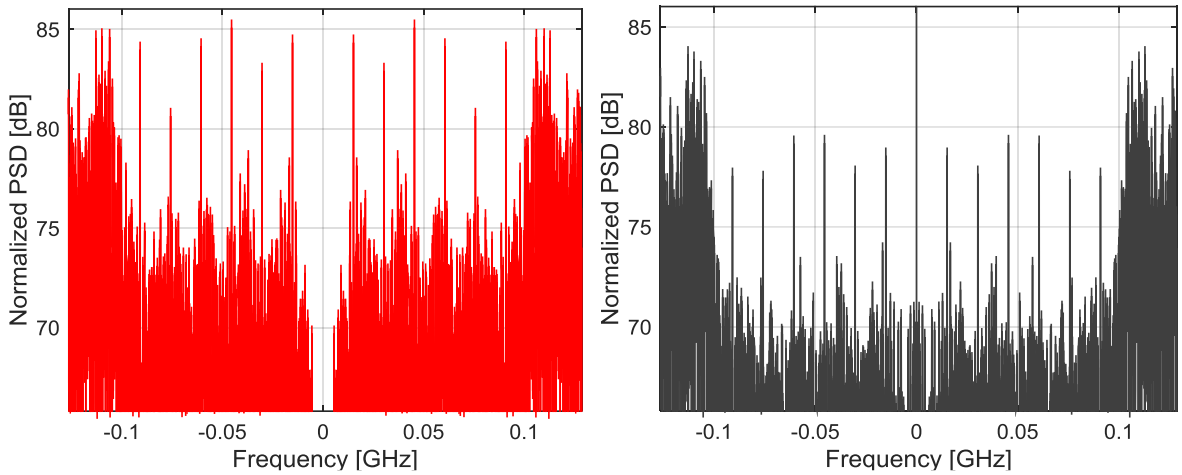

Figure 3.4 – (Left) Input of the DSP, zoomed in at the SSBI component. (Right) Output of the DSP, zoomed in at the SSBI mitigated with MP.

The constellation at the receiver output for the complete MP structure from table 3.7 is represented in figure 3.5. The constellations obtained for the past and future MP are similar to the one obtained for the complete MP.

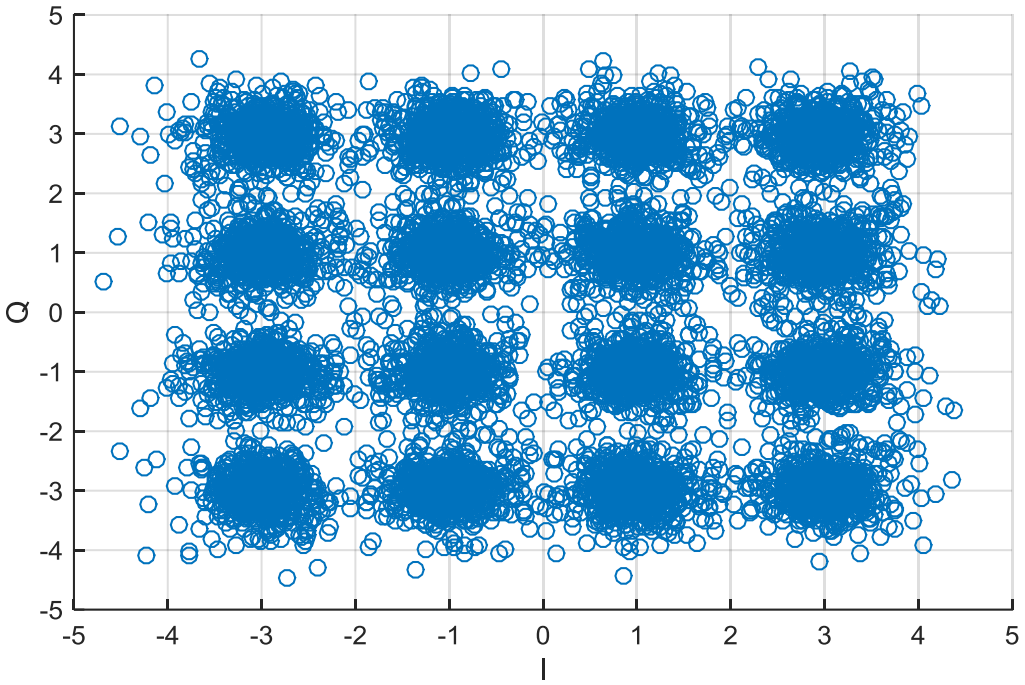

Figure 3.5 - Constellation at the receiver when the complete MP is used to mitigate SSBI.

3.4 Evaluation of the importance of the coefficients

In section 3.3, the best structures of MP were obtained. Each one of them uses a large quantity of coefficients, which increases the computer complexity of the system. In order to reduce this complexity, each structure was tested with the objective of determining if all the coefficients of the same structure were important. If any coefficient was to be considered not important than it could be ignored and therefore decrease the computer complexity. The test used the parameters from table 3.1 and the same input symbols used to obtain the results of the extensive test from section 3.3. In this test, each coefficient, one by one, was forced to zero and then the value of the EVM was calculated, in order to determine if that coefficient was important or if it could be discarded. Figure 3.6 represent the results of this test, for the complete MP structure.

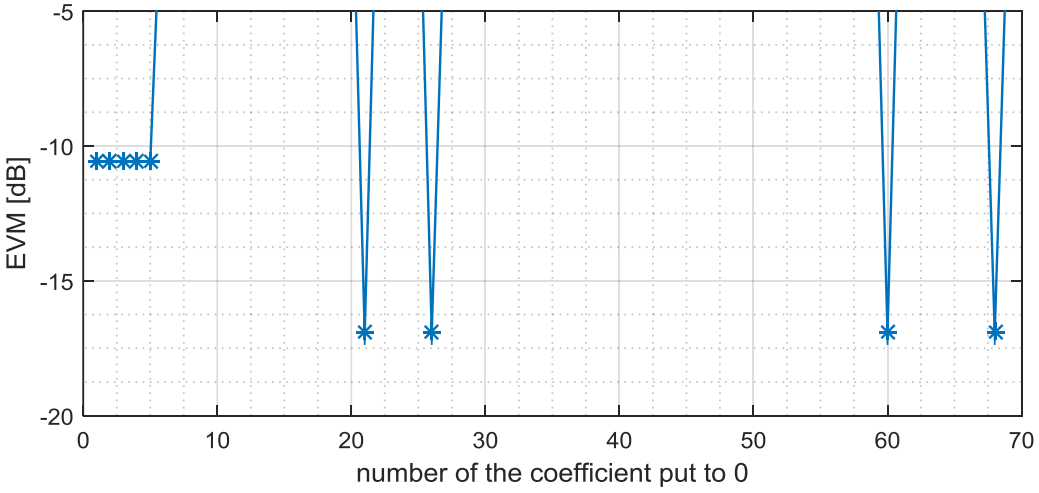

Figure 3.6 - Assessment of the importance of the coefficients of the complete MP.

Figure 3.6 shows that the coefficients from the complete MP structure are all important. This conclusion is verified by the fact that when each coefficient is forced to zero, the EVM instead of being approximately equal to the values presented in table 3.7 for the complete MP, became approximately -10 dB for the initial coefficients and 2 dB for the rest of them. The only cases in which the EVM remained unchanged were for the coefficients that were zero before this test was executed. This test was done for the past and future MP and the result was similar.

3.5 Adaptive iteration method

In previous test, the performance achieved was obtained with a certain sequence of OFDM symbols that originated an optimal value for the coefficients estimated. However, when random sequences of OFDM symbols are used, the coefficients obtained are different from the optimal and therefore the performance obtained is not the same. Although the MP structures chosen can achieve acceptable performance results when random symbols are used, the randomness of the OFDM symbols sometimes result in cases of poor performance. To prove this, each of the MP structures chosen in section 3.3 was tested with the same 200 OFDM symbol sequences, different from the ones used in section 3.3. In figure 3.7 it is represented the result obtained for this test for the complete. Each test was performed using the parameters from table 3.1**.**

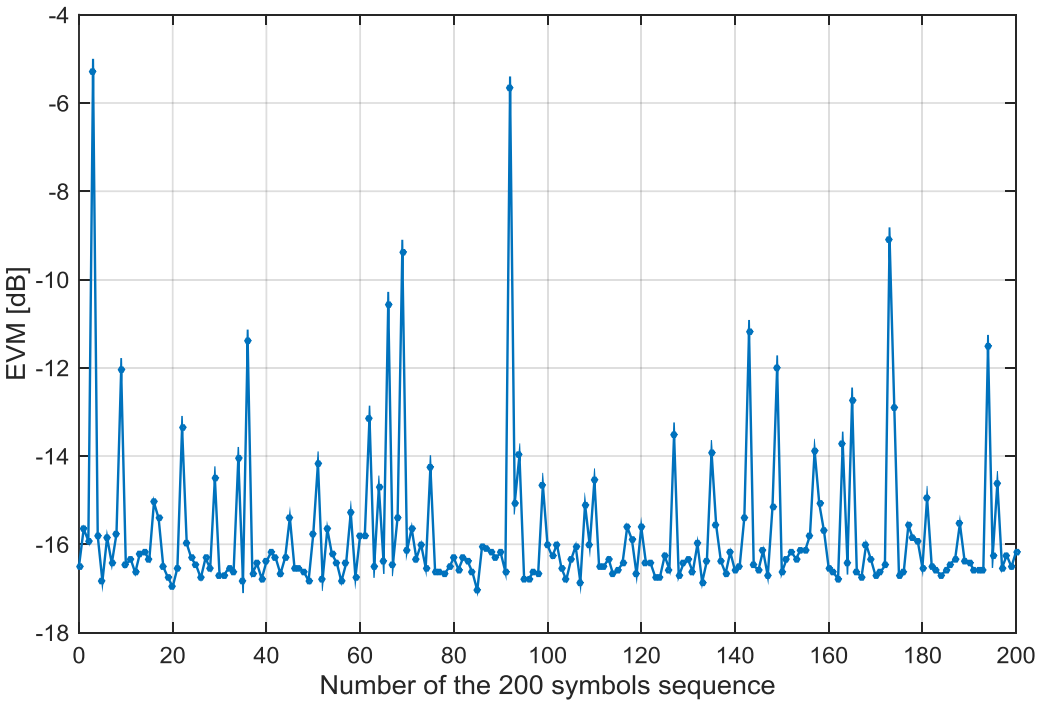

Figure 3.7 - EVM obtained using the complete MP with 200 OFDM symbol sequences.

Through observation of figure 3.7, it is possible to conclude that for some OFDM symbol sequences, the complete MP structure achieved an acceptable performance (below -16 dB of EVM). However in other cases this did not happen. For example, for OFDM symbol sequence number 3, the EVM obtained

at the receiver is higher than the EVM obtained when no SSBI mitigation is used. This problem occurs because the coefficients of the MP are estimated based on the part of the signal that corresponds to the training symbols and the EVM is calculated using the information symbols. If the coefficients were to be estimated based on the information symbols, then the performance of the system would increase significantly. This conclusion can be corroborated through figure 3.8, in which it is represented the case from figure3.7 but with the result obtained when the coefficients are estimated using the information symbols.

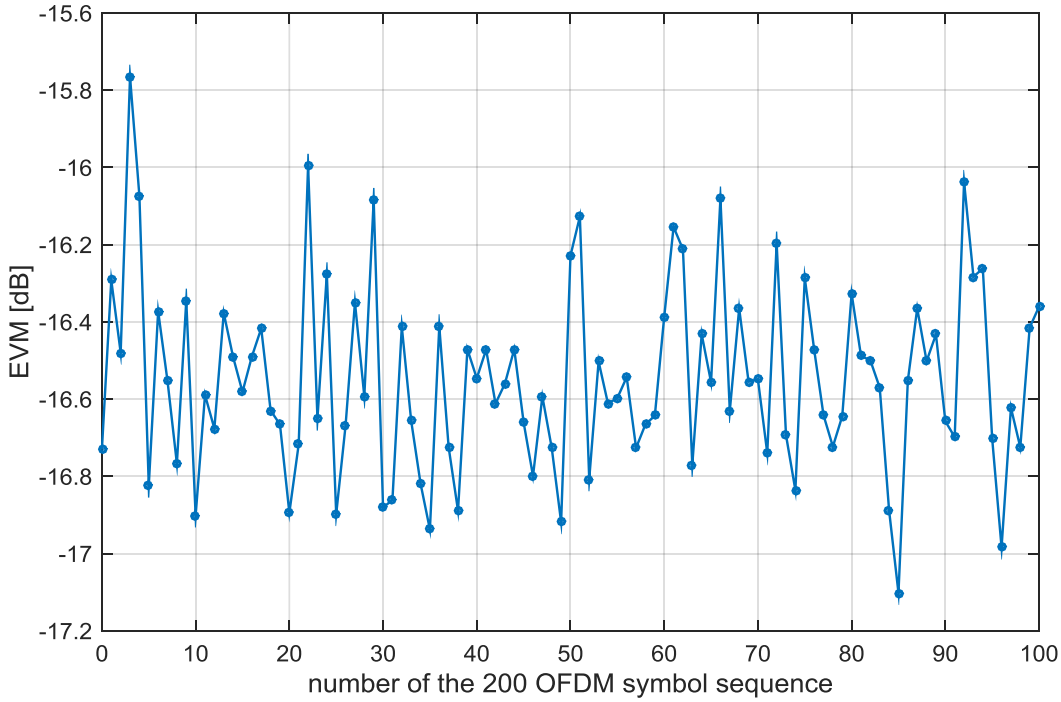

Figure 3.8 - EVM obtained when the MP coefficients are estimated using the information symbols, for the complete MP.

To try and solve this problem, a technique proposed in [22] was used which relies on the update of the coefficients. Since the structure of the MP cannot be changed, the coefficients of the MP have to be updated in order to withstand the different OFDM symbols sequences that are used in the system. This update can be done through an adaptive technique as it is proposed in [22] and the values of (i+1)-th estimate of **w** are given by

$$\mathbf{w}_{i+1} = \mathbf{w}_i + \mu \cdot \left(\mathbf{V}^{\mathrm{H}}\mathbf{V}\right)^{-1}\mathbf{V}^{\mathrm{H}}\left(\boldsymbol{x} - \mathbf{V}\mathbf{w}_i\right) \tag{3.13}$$

where μ is the relaxation constant. The update performed on the coefficients with expression (3.13) is achieved by calculating the error between the signal from the transmitter x and the approximation that is calculated through $\boldsymbol{V}\boldsymbol{w}_i$, where $\boldsymbol{V}$ is the matrix from expression 3.6 and $\boldsymbol{w}_i$ are the coefficients from the previous iteration. This error is then multiplied with $\left(\mathbf{V}^{\mathrm{H}}\mathbf{V}\right)^{-1}\mathbf{V}^{\mathrm{H}}$, which is $\mathbf{V}^{-1}$, in order to obtain the value of the coefficients associated to the error. This correction value is then multiplied with the relaxation constant and then summed to the value of the previous coefficients. This operation is intended

to be executed one time, each time the input OFDM symbol sequence changes and the value of the relaxation constant, according to [22], μ has to be inferior to one. To correctly determine the adequate value for the relaxation constant, different values for the relaxation constant were tested. The results are presented in the next section, section 3.5.1.

3.5.1 Determination of the relaxation constant

The relaxation constant, as it was introduced at the end of section 3.5, has to be inferior to one. Choosing the value of this constant has two possible outcomes. On one hand, if the value is big, then the coefficients would rapidly converge to the optimal value, but this would lead to an unstable convergence because, since the μ value is big, the coefficient values would vary too much, which could also lead to no convergence at all. On the other hand, if the μ value is small, the unstable problem of the high value of μ would not occur, but the convergence would be slower. The typical value used, according to [22] is 0.1. To determine the optimal value of μ, each MP structure was tested for a μ between 0 and 0.5. In this test, 200 sequences of OFDM symbols were used (the same used in the test from section 3.5) for each MP structure. The sequences were the same for the three MP structures tested. The system parameters were the same from table 3.1. In figure 3.9, it is represented the result of this test, in which it is represented the difference between the maximum and the minimum values of EVM obtained for each value of the relaxation constant.

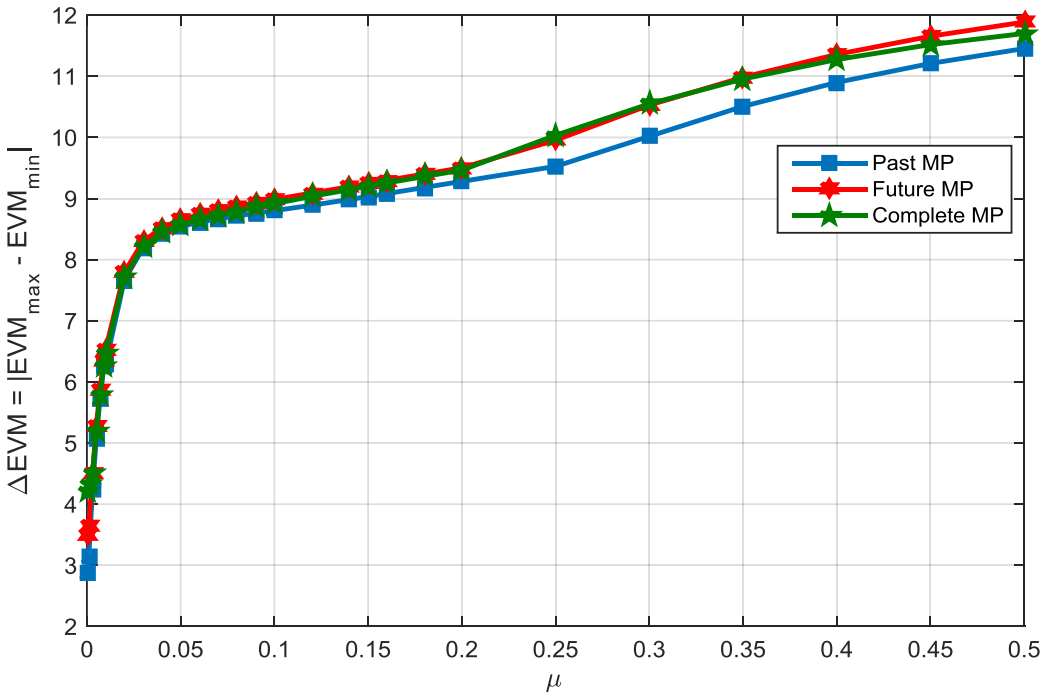

Figure 3.9 - EVM variation between maximum and minimum value for each relaxation constant value.

The graph obtained in figure 3.9 does not provide any help in choosing the best relaxation constant. This happens because it shows that the best value for μ is 0, which results in a difference of EVM of just

2 dB and results in a smooth variation of EVM through the 200 sequences. This smooth variation can be verified in figure 3.10 for the case of the complete MP.

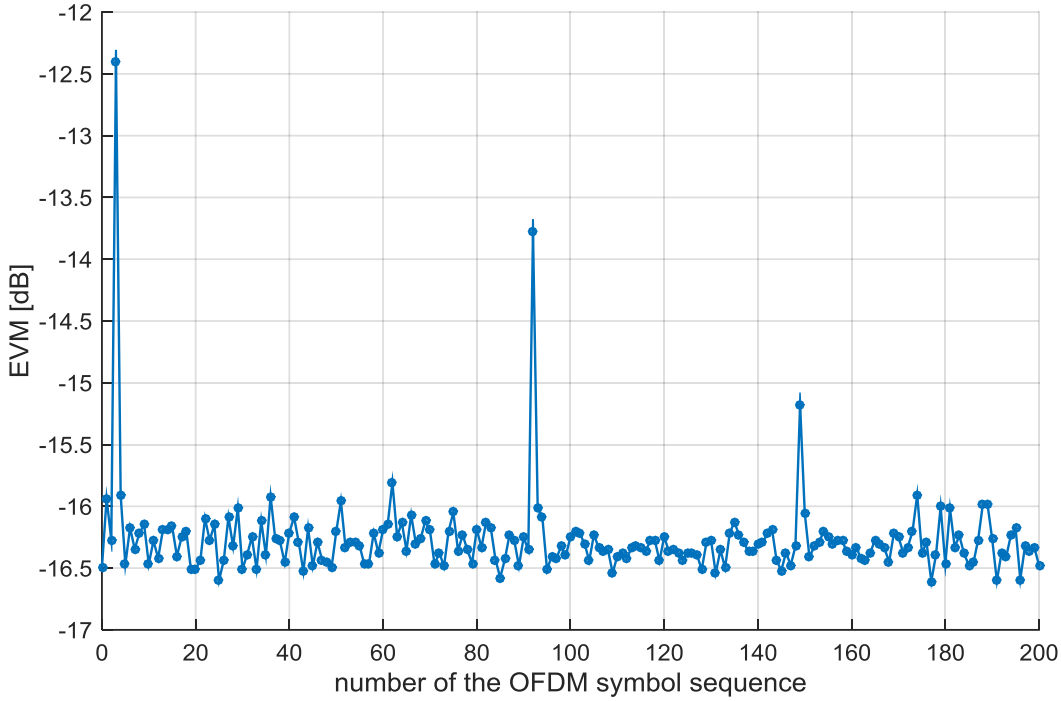

Figure 3.10 - EVM obtained when the complete MP uses a relaxation constant of 0.

The reason why this extensive test depicts that the best value for μ is 0 is because of the first 200 OFDM symbol sequence. Since the first sequence is similar to the optimum sequence from section 3.2, the coefficients don't need any update at all. With the increase of the μ value, the coefficients values deviate from there optimum value, which leads to an increase on the difference of EVM. So the figure 3.9 (Delta EVM) does not provide any conclusion regarding the choice of μ, it helps concluding that the three MP considered in section 3.2 have similar behaviours. Therefore from now on the MP chosen to the upcoming tests is the complete MP. This choice was made because this MP uses less coefficients (Complete - 87, Future - 106, Past - 110) when compared to the others which results in less computer complexity and faster simulations.

In order to conclude which would be the optimum value for the relaxation constant, the first OFDM symbol sequence was changed. This was done maintaining the original 200 OFDM symbol sequences and only shifting their order. This action was done 7 times (starting in sequence 3, 8, 10, 16, 25, 100 and 150) and the values for the μ were different from the first test. Instead of varying the μ from 0 to 0.5 the test was performed for the following values:

[0 0.001 0.003 0.005 0.007 0.01 0.02 0.03 0.05 0.07 0.1]

Also, instead of just representing the difference between the maximum and the minimum values of EVM like in figure 3.9, it was also calculated the mean BER from the values of EVM obtained through the expression from appendix A.5. Also, in the graphs with the mean BER, it was also included the values of the worst (in orange) and best (in yellow) mean BER possible to achieve. The worst value belongs to the case where the adaptive is not used (represented in figure 3.7) and the best case belongs to the case where the coefficient estimation and the EVM calculation is performed on the same symbols. Considering these parameters and the system parameters from table 3.1 the results obtained were the following:

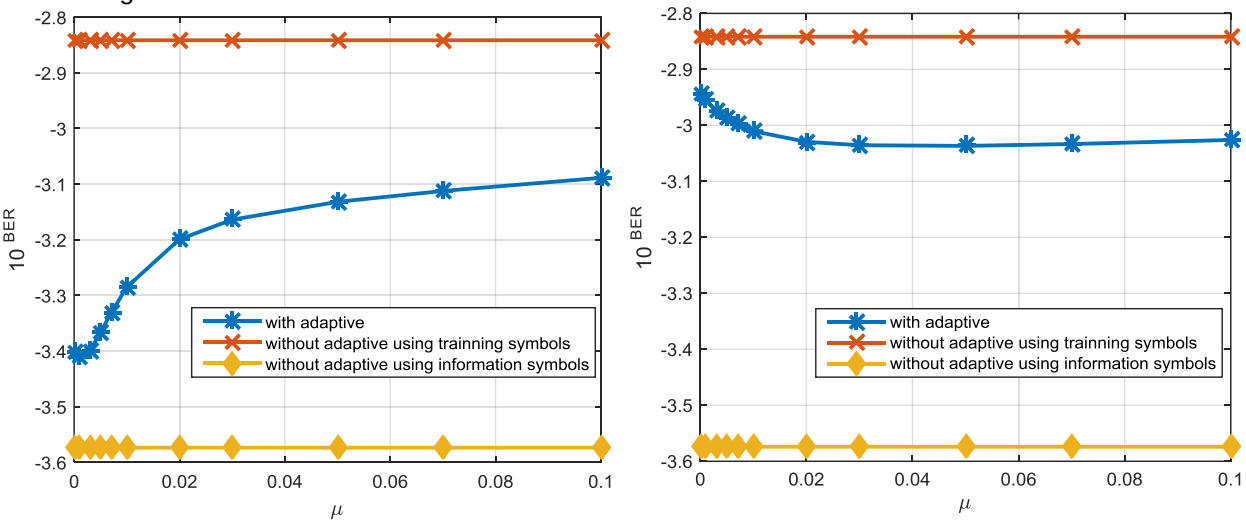

Figure 3.11 - On the left, BER obtained for the original OFDM symbol sequence as the first one. On the right the OFDM symbol sequence 3 as the first one. In both graphs it is represented, in this order, the results without adaptive using the training symbols for coefficient estimation, with adaptive and without adaptive using the information symbols for coefficient estimation.

The remaining 6 cases are similar to the two different cases from figure 3.11. When looking at the 8 cases obtained by calculating the mean BER value, the conclusion is that when the first sequence is similar to the optimal (figure 3.11 left), the use of adaptive with μ = 0 increases the value obtained for the BER. When the first sequence is not similar to the original one (figure 3.11 right), the use of adaptive with μ > 0 tends to reduce the BER achieved. In both cases, the increase on BER or decrease on BER is not significant. Therefore, the use of adaptive with μ > 0 does not bring any advantage. It tends to add computer complexity, without improving the BER signal when compared to the case without adaptive. So the choice is to adaptive with μ = 0, which means that the coefficients used on the first estimation stay untouched.

3.6 Behaviour of the MP structure chosen to VBG, VBPR and modulation index

In this section, the behaviour of the complete MP structure, was analysed when the parameters VBG, VBPR and m were changed. The system parameters used in this test were the same from table 3.1 and the OFDM symbols used were the same from the test that lead to the choice of the MP structures in section 3.3. In each analysis, it is represented a figure with the EVM in function of the parameter put to the test when the MP mitigation is used and when no SSBI mitigation is used. Also, when each parameter is being tested, the other two maintain the value from table 3.1.

3.6.1 Variation of the VBG

SB

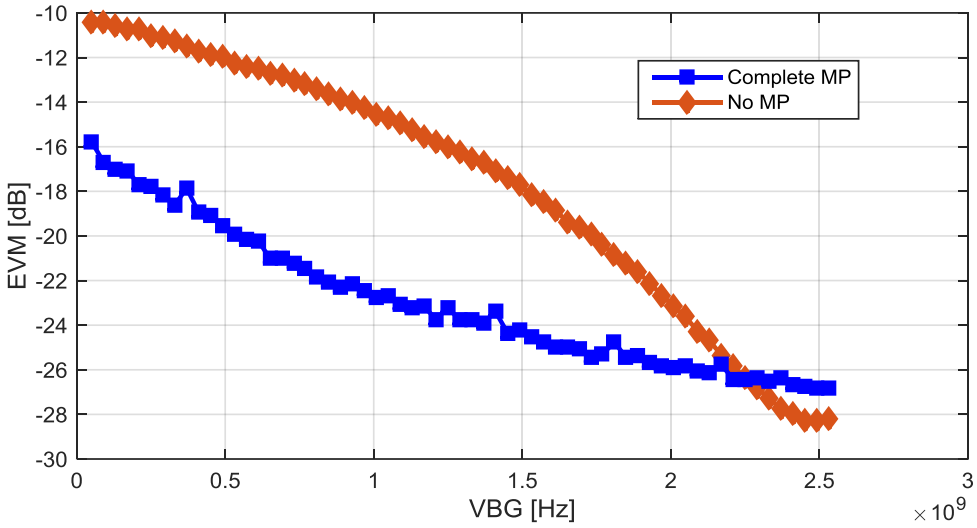

Figure 3.12 - EVM variation with VBG for SB.

Comparing the two, when the VBG increases, the OFDM band gets less affected by the SSBI, until it does not interfere with the band when the VBG is equal to the OFDM band bandwidth. However, there is a slight difference between the two cases (with or without MP). The difference is that the EVM obtained is better with the MP. This happens because, when the VBG is lower than the OFDM band bandwidth, the MP mitigate the SSBI which is the main distortion effect.

MB

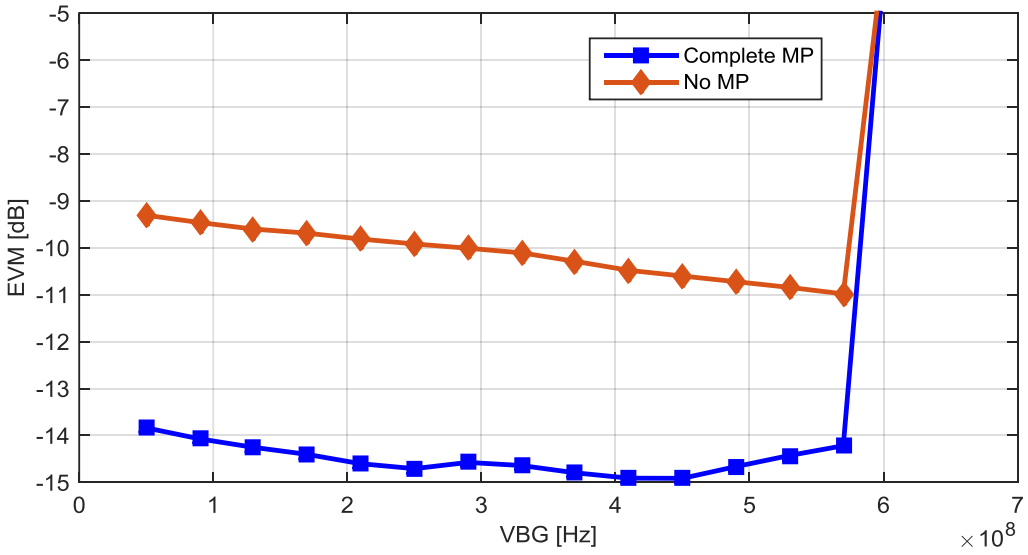

Figure 3.13 - EVM variation with VBG for MB.

When comparing the two cases, with MP or without, the difference lies in the EVM achieved, being lower when the MP is used because it mitigates the SSBI. In both cases the maximum VBG that can be used is equal to the gap between consecutive bands. For example, the first band has a central frequency of 2 GHz and consecutive band a central frequency of 5.125 GHz. Since the bandwidth of the OFDM band is 2.5 GHz, then the gap between bands is 625 MHz. In figure 3.13 the limit VBG is lower, 570 MHz.

This difference occurs because of the margin used in the ideal filters around the simulator developed. Once this limit is surpassed, overlap of bands occur and the performance of the system is affected negatively.

3.6.2 Variation of the VBPR

SB

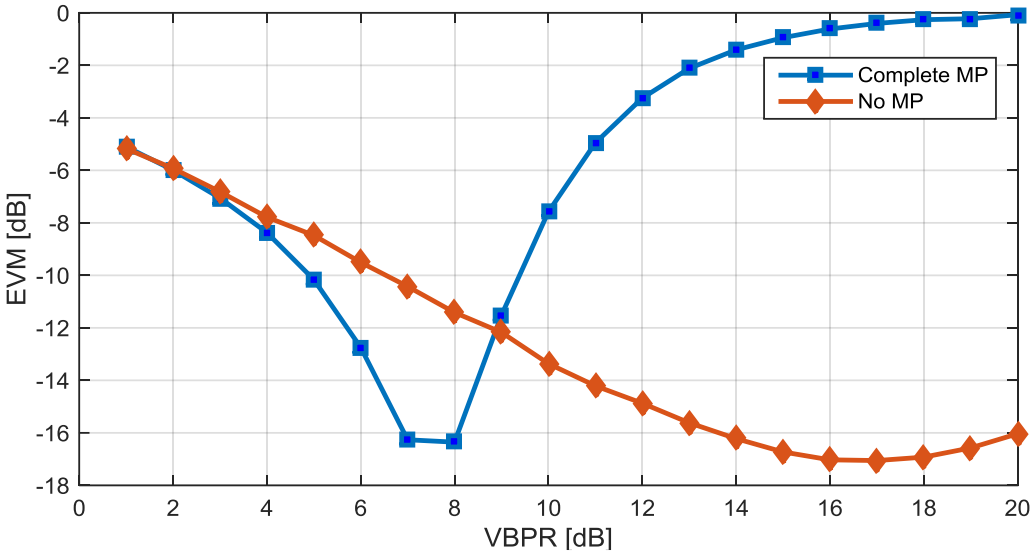

Figure 3.14 - EVM variation with VBPR for SB.

When comparing the two cases, the case without MP has optimal value of VBPR around 17 dB. When the MP is used, the optimal value is lower, around 8 dB. This happens because, since the SSBI term is mitigated, the ratio between the signal power and the virtual carrier needs to be smaller to achieve the same EVM value. When no mitigation is used, in order to reduce the effect of the SSBI, the power of the virtual carrier needs to be relatively higher than the power of the OFDM signal, which leads to a higher VBPR.

MB

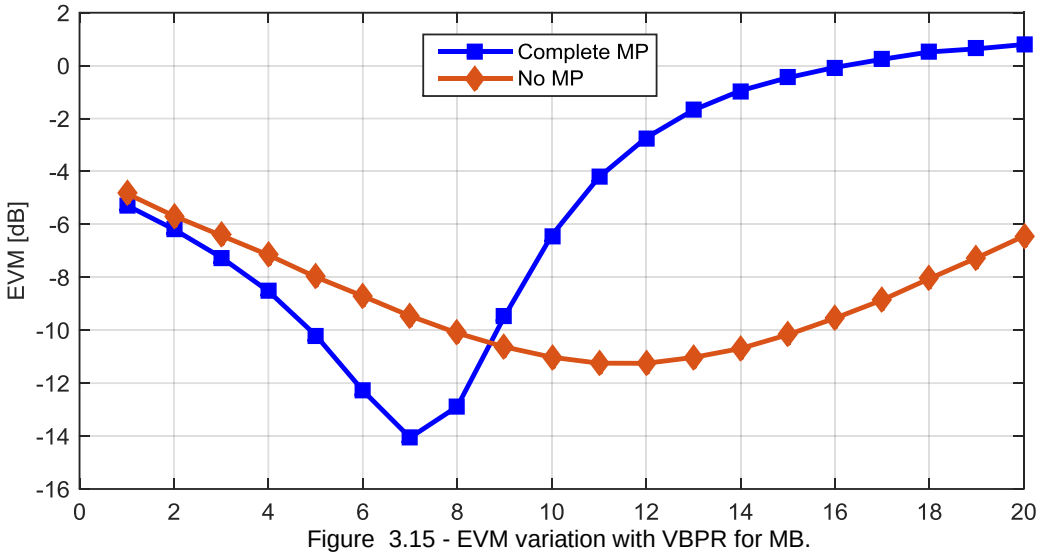

Figure 3.15 - EVM variation with VBPR for MB.

In MB the behaviour is similar to the one in SB, when MP is not used the optimal VBPR is higher than when the MP is used.

3.6.3 Variation of the modulation index

SB

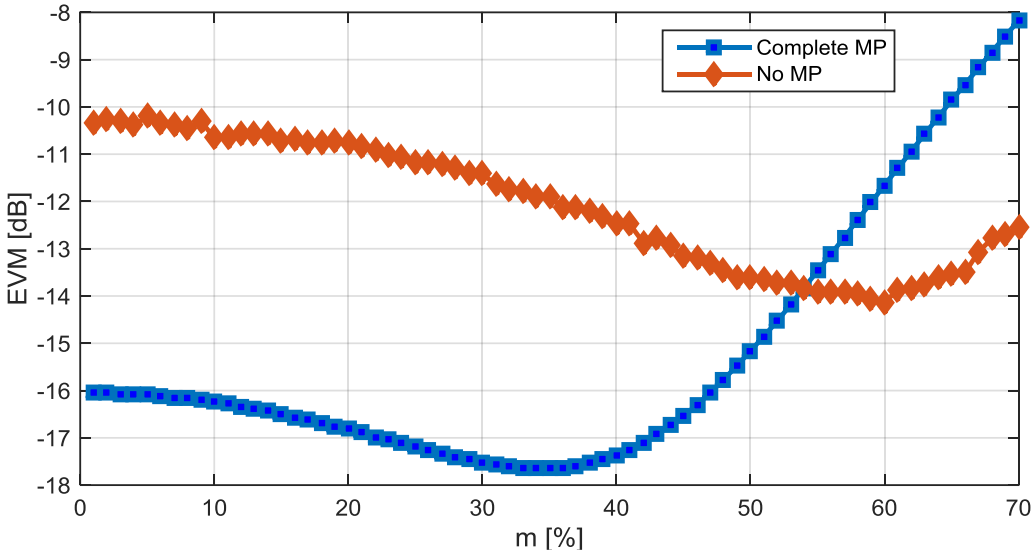

Figure 3.16 - EVM variation with m for SB.

In single band, the optimal value of modulation index is around 60% and when MP is used is around 35%, but with a lower value of EVM. This happens because with only one band the MP is able to mitigate the nonlinearities of the DP-MZM. The nonlinearities of the DP-MZM are important when the modulation index is high. When the modulation index is lower, the distortion that interferes with the signal is the noise.

MB

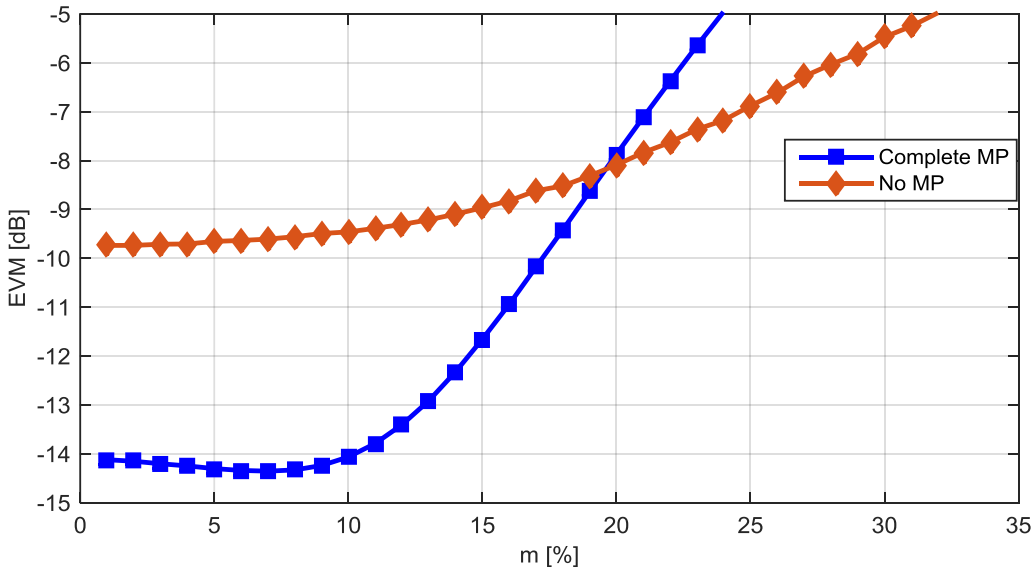

Figure 3.17 - EVM variation with m for MB.

In multi band, the nonlinearities of the DP-MZM for higher values of m are more explicit because they interfere between OFDM bands. Therefore in MB the nonlinearities of the DP-MZM are worse than the noise because the MP cannot mitigate these nonlinearities like it was able in SB. Therefore the lower

value of m is optimal, around 7-10%. When the MP is not used the behaviour is the same but with higher EVM, because the SSBI is not mitigated.

Conclusion regarding the modulation index: when choosing the value of *m* there are two distortions that are important to refer, the distortion induced by the DP-MZM and the noise. When the value of m is low the distortion of the DP-MZM is low because the DP-MZM is as similar as a linear MZM. When the value of m is higher, the impact of the DP-MZM is higher than the noise. In SB, since there is no interference between bands, the distortion of the DP-MZM is mitigated by the MP which makes the impact of the noise considerable to the impact of the mitigated DP-MZM distortion. In MB, the distortion of the DP-MZM has a higher impact than the noise because of the interference between bands which makes the values of m the lower the better.

3.7 Band selector

The band selector plays an important role in an MB system because it allows the selection of a certain band or group of bands to be processed. In the tests so far, the band selector used was an ideal filter, which only exists in simulations. So, it is important to use a band selector that correctly describes a real filter used in real MB-OFDM systems. The filter that is ought to be used in this work is the second order super Gaussian filter [56]. When comparing the second order super Gaussian filter to the ideal filter its selectivity is lower than the ideal one.

The selectivity is the ratio between the bandwidths of the filter at -3 dB and -20 dB.

$$S_f = \frac{B_{-3dB}}{B_{-20dB}}, \quad S_f \in [0,1]. \tag{3.14}$$

Since the ideal filter is a rectangle, its selectivity is 1 because the bandwidth at -3 dB is equal to the bandwidth at -20 dB. The second order super Gaussian filter has a selectivity of 0.62 (confirm with calculations), which means that the bandwidth at -3 dB is approximately 62 per cent of the bandwidth at -20 dB.

Since the 2nd order super Gaussian filter is not linear, it is necessary to choose its parameters correctly so that its usage does not interfere much with the performance of the system. In other words, the bandwidth of the filter cannot be too small leading to a cut of the OFDM band or too high and select the OFDM band and its adjacent bands. The filter parameters are the central frequency, the filter bandwidth at -3 dB and the detuning of the filter. The central frequency needs to be equal to the centre of the group composed by the OFDM band and the virtual carrier and the filter bandwidth needs to be equal to the bandwidth of the OFDM band. The detuning needs to be adjusted. Detuning represents the deviation of the filter from the centre of the OFDM bandwidth. Therefore a detuning of 0 Hz means that the filter is tuned with the centre of the OFDM band. According to [56] a correct value to use for detuning in the MORFEUS MB-OFDM system is 300 MHz. In figure 3.18 there is represented the spectrum of a 3 band system, where the second band is selected. The parameters used in this test are represented in table 3.1.

The parameters of the band selector are 2.2 GHz for the -3dB bandwidth and the central frequency was equal to the central frequency of the 2nd band (5.125 GHz) plus the detuning of 300 MHz.

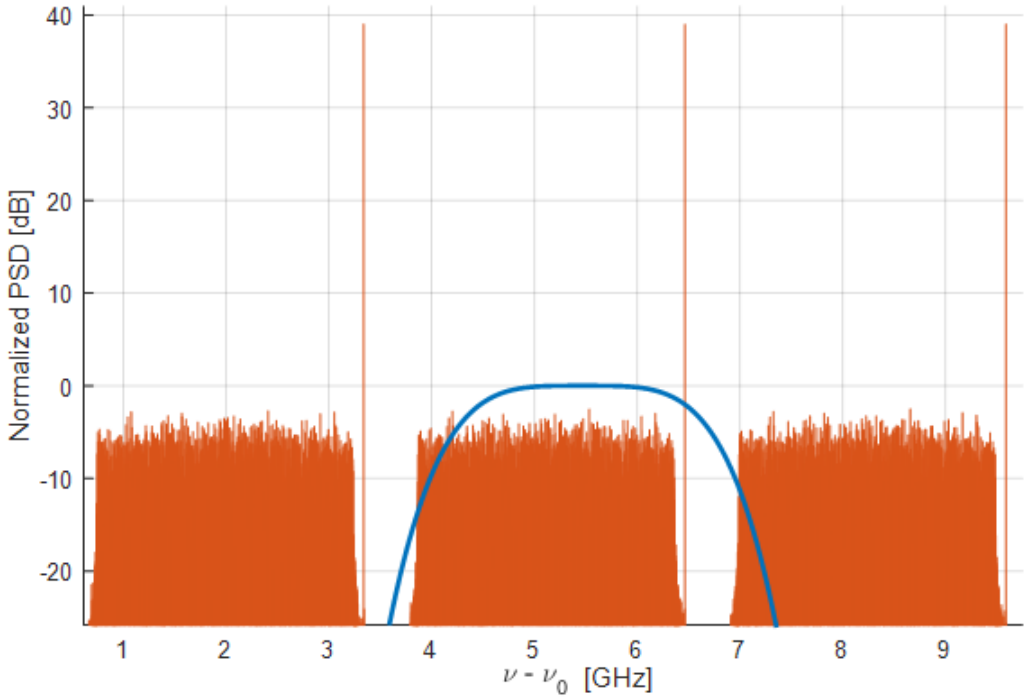

Figure 3.18 - Spectrum of the 2nd order super Gaussian filter selecting an OFDM band with central frequency of 5.125 GHz.

Although the band selector selects part of the adjacent band, because of the 300 MHz of detuning, with this value for detuning the system is able to select more power of the virtual carrier. By selecting more power of the virtual carrier, the down-conversion is more efficient and allows the system cross talk to be lower.

3.8 Conclusions

In this chapter, the theory of memory polynomials was introduced. The structure of the MP used to mitigate the SSBI was described and the best structures that allowed an improvement on the system performance were accessed. It was concluded that with the structures defined, the system performance would improve and therefore decrease the effect of the SSBI in the system.

The method of the adaptive, which was intended to update the coefficients of the MP, was presented and the variables of this method were studied. It was concluded that this method did not bring any advantage to the system performance, therefore being discarded.

The values of the parameters VBPR, VBG and modulation index were studied when MP mitigation is used and compared to when no mitigation of SSBI is used.

The band selector used on the MB-OFDM system was presented and its parameters were defined.

Chapter 4 - Performance evaluation of MB-OFDM system employing MP for SSBI mitigation

In this chapter the MB-OFDM system described in section 2.3 is assessed to determine the minimum required OSNR to achieve a BER of 10^{-3}, when the MP described in chapter 3 is used to mitigate the SSBI.

4.1 Introduction to the tests performed

The main objective of this work is the mitigation of the SSBI distortion. However, there are other sources of distortion present on the MB-OFDM system, like the electrical-to-optical modulator (the DP-MZM in this work) introduced on section 2.2.3, the band selector (2^{nd} order super Gaussian model) which parameters were defined in section 3.7 and the transmission medium (SSMF optical fibre), presented in section 4.3. The performance impact caused by the band selector and transmission medium are to be evaluated in further detail in this chapter.

This evaluation is supported by the determination of the EVM and BER values for each band of the MB-OFDM system. The BER is calculated using the exhaustive Gaussian approach (EGA), which allows its value to be estimated using different values of noise, increasing the accuracy of the results. With these calculations, it is determined if it is possible to achieve a BER of 10^{-3} and if doing so, what is the minimum required optical signal-to-noise ratio (OSNR).

To determine this minimum required OSNR, four different evaluations were conducted, each one focusing on the impact of a not ideal component present on the MB-OFDM system. As introduced in the beginning of this chapter, the not ideal components considered were the 2^{nd} order super Gaussian filter used on the band selector and the SSMF optical fibre used in the transmission channel. The four evaluations, which results are discussed on the next sections and presented on appendix B, were divided into two sections. In section 4.2, the impact of the 2^{nd} order super Gaussian filter was compared to an ideal filter in optical back to back and in section 4.3 this impact was evaluated with the SSMF optical fibre.

The tests were performed using a SB system and MB system. Each system was designed using the parameters described in section 2.3.5. Regarding the 2^{nd} order super Gaussian filter, the BS bandwidth, central frequency and detuning were defined according to section 3.7. Compared to the tests performed on chapter 3, where the analysis was done noise free, the study performed on chapter 4 considered the two types of noise, electrical (appendix A.2) and optical noise (appendix A.6). The parameters used on these tests were similar the parameters from table 3.1. Except for the symbol period, cyclic prefix and bitrate which are from section 2.3.5 and the number of chip samples which was 64. The results for these tests are represented in appendix B1, B2, B3 and B4. For each MB test, the value for the OSNR represented was the one that achieved the lower BER.

4.2 Performance evaluation in optical back-to-back

4.2.1 Band selector employing ideal filter in optical B2B

This first case was designed to evaluate what was the system performance when the least introduction of distortion was done on the system. This meant using the ideal band selector and a B2B configuration. The ideal band selector is composed by a filter that can only be produced via computer simulation since it represents a rectangle (selectivity equal to one). Although this ideal filter is used in other locations of the MB-OFDM system (for example in the transmitter after the up-conversion, section 2.1.5) and has a small/almost negligible impact on the system performance, it is referred in this section to be compared with the impact on the system performance caused by the 2nd order super Gaussian filter. The results for this test are represented in table 4.1 for SB and 4.2 for MB.

Table 4.1 - Results for ideal band selector in optical B2B, SB.

SB - B2B	
OSNR [dB]	32.75
10^{BER}	-2.115
EVM [dB]	-16.07

Table 4.2 - Results for ideal band selector in optical B2B, MB.

MB - B2B												
Band	**1**	**2**	**3**	**4**	**5**	**6**	**7**	**8**	**9**	**10**	**11**	**12**
OSNR [dB]	40	40	39	39.5	37	39.25	40	32.5	39.25	40	34.25	37
10^{BER}	-1.95	-2.39	-1.84	-1.94	-2.18	-2.2	-1.96	-2.27	-2.51	-2.19	-2.09	-2.78
EVM [dB]	-15.5	-14.8	-14.8	-15.2	-14.3	-13	-10.5	-14.7	-14.9	-14.5	-15.2	-13.1

Through observation of table 4.1 it is possible to conclude that the lowest BER achieved is higher than 10^{-3}, leading to the conclusion that these SB system with MP mitigation on the DSP is not capable of mitigating the distortions introduced on the system.

Table 4.2 show the results for the MB configuration. In this case only the band 12 is capable of achieving a value near 10^{-3}. So, also for this case, it is not possible to achieve the 10^{-3} of BER. In this case, this is caused by the crosstalk between bands and also by the harmonics from the other bands that introduce distortion that the MP cannot mitigate.

4.2.2 Band selector employing 2nd order super Gaussian filter in optical B2B

In this second case, instead of the ideal filter on the band selector, it was used the 2nd order super Gaussian filter introduced in section 3.7. This filter used a cut frequency of 2.2 GHz with a detuning of 300 MHz to increase the power of the virtual carrier that is selected in order to help the photodetection. The increase of power of the virtual carrier helps neglect the effect of the 2nd order term of equation 2.28. The 2nd order super Gaussian filter has a high impact on the system performance, especially on the MB configuration. This occurs because during the selection of a certain band, since this filter is not rectangular (selectivity is inferior to one), it is selected more than the OFDM signal which cases distortion. On the case of the SB configuration, the distortion introduced is less because there are no adjacent bands. However it still adds noise to the system which is unsatisfactory. The results for SB are represented in table 4.3 and for MB in table 4.4.

Table 4.3 - Results for 2nd order super Gaussian band selector in optical B2B, SB.

SB - B2B	
OSNR [dB]	35.5
10^{BER}	-1.88
EVM [dB]	-15.7

Table 4.4 - Results for 2nd order super Gaussian band selector in optical B2B, MB.

MB - B2B												
Band	**1**	**2**	**3**	**4**	**5**	**6**	**7**	**8**	**9**	**10**	**11**	**12**
OSNR [dB]	39.25	40	40	34	40	38	40	35.5	40	40	39.5	38.25
10^{BER}	-1.76	-2.2	-1.67	-1.8	-2.16	-1.95	-1.85	-2.09	-2.16	-2.1	-2.03	-2.68
EVM [dB]	-14.5	-14.4	-13.9	-14.1	-14	-12.6	-10.2	-14.5	-14.2	-13.4	-14.8	-15.1

Once again it is not possible to achieve the BER of 10^{-3}. It is also not possible with MB configuration.

4.3 Performance evaluation with SSMF model

So far, the previous tests were performed in optical back to back configuration, where the output of the transmitter was considered to be directly connected to the input of the receiver. However, metro networks are not designed using this type of configuration. Therefore, it is important to analyse the impact of the transmission medium on the system. The transmission medium used in optical communications systems are optical fibres the used on the system of this work is the SSMF, presented in section 2.3.7.

4.3.1 Band selector employing ideal filter with SSMF model

In this 3rd case, the impact of the optical fibre in system performance was evaluated. To first determine this impact alone, the band selector used the ideal filter. As introduced in section 4.1, this test was performed for four different fibre lengths, 100 to 400 kms to evaluate the dispersion and attenuation introduced on the system. However, since the results were similar for the four lengths considered, only the shortest and longest were displayed. In tables 4.5 and 4.6 there are represented the EVM and BER for SB and in table 4.7 and 4.8 the results for MB.

Table 4.5 - Results for ideal band selector with SSMF model (Lf=100km), SB.

SB - Lf = 100 km	
OSNR [dB]	34
10^{BER}	-2.1
EVM [dB]	-16.09

Table 4.6 - Results for ideal band selector with SSMF model (Lf=400km), SB.

SB - Lf = 400 km	
OSNR [dB]	34
10^{BER}	-2.11
EVM [dB]	-16.09

Table 4.7 - Results for ideal band selector with SSMF model (Lf=100km), MB.

MB - Lf = 100 km												
Band	**1**	**2**	**3**	**4**	**5**	**6**	**7**	**8**	**9**	**10**	**11**	**12**
OSNR [dB]	38.25	38	36	36	34	38	39.5	37	39	40	34	36.5
10^{BER}	-1.95	-2.41	-1.84	-1.94	-2.15	-2.17	-1.96	-2.25	2.5	-2.19	-2.1	-2.75
EVM [dB]	-15.4	-14.76	-14.76	-15	-14.25	-12.96	-10.2	-15.1	-14.9	-14.6	-15.2	-13.6

Table 4.8 - Results for ideal band selector with SSMF model (Lf=400km), MB.

MB - Lf = 400 km												
Band	**1**	**2**	**3**	**4**	**5**	**6**	**7**	**8**	**9**	**10**	**11**	**12**
OSNR [dB]	38	40	39.25	34	36.5	38	40	32.75	39.25	40	36	36.5
10^{BER}	-1.95	-2.38	-1.84	-1.93	-2.19	-2.2	-1.95	-2.27	-2.55	-2.17	-2.08	-2.8
EVM [dB]	-15.4	-14.8	-14.9	-14.8	-14.3	-12.9	-10.3	-14.8	-14.9	-14.6	-15.26	-13.2

Analysing the four groups of results, neither of them present a BER lower or equal to 10^{-3}, meaning that the system cannot achieve that result. Also by looking at the impact of the optical fibre on the system EVM, it is seen that it does not affect the system. This happens because the time spread, t_d, is inferior to the CP which is calculated taking into account the length of the optical fibre. This results in an ISI and ICI free signal. This also occurs for the MB-OFDM signal, the impact of the optical fibre is not considerable and there is no band where the OSNR is capable of achieving 10^{-3}. This conclusion is supported by results from tables 4.7 and 4.8.

4.3.2 Band selector employing 2nd order super Gaussian filter with SSMF model

At last, the 4th test that represents the best approximation to the real system, where the band selector has the 2nd order super Gaussian filter and the optical fibre implemented. Since this system case considered the distortions introduced on the system by the band selector and the optical fibre and since the other cases were not able to achieve the 10^{-3} BER mark with any value of OSNR, this case was already expected to perform poorly as well. As referred in section 4.3.1, since the results were similar for the four lengths considered, only the results for the shortest and longest fibre length were displayed. Tables 4.9 and 4.10 contain the EVM and BER for SB and tables 4.11 and 4.12 the results for MB.

Table 4.9 - Results for 2nd order super Gaussian band selector with SSMF model (Lf=100km), SB.

SB, Lf = 100 km	
OSNR [dB]	33.75
10^{BER}	-1.88
EVM [dB]	-15.69

Table 4.10 - Results for 2nd order super Gaussian band selector with SSMF model (Lf=400km), SB.

SB, Lf = 400 km	
OSNR [dB]	32.5
10^{BER}	-1.88
EVM [dB]	-15.67

Table 4.11 - Results for 2nd order super Gaussian band selector with SSMF model (Lf=100km), MB.

MB, Lf = 100 km												
Band	**1**	**2**	**3**	**4**	**5**	**6**	**7**	**8**	**9**	**10**	**11**	**12**
OSNR [dB]	39.25	36.75	39.5	33.25	40	35	40	39.5	40	37	39	39.5
10^{BER}	-1.75	-2.19	-1.67	-1.81	-2.16	-1.94	-1.85	-2.1	-2.15	-2.08	-2.02	-2.7
EVM [dB]	-14.5	-14.3	-13.8	-14.1	-14.0	-12.4	-10.1	-14.4	-14.3	-13.4	-14.8	-15

Table 4.12 - Results for 2nd order super Gaussian band selector with SSMF model (Lf=400km), MB.

MB, Lf = 400 km												
Band	**1**	**2**	**3**	**4**	**5**	**6**	**7**	**8**	**9**	**10**	**11**	**12**
OSNR [dB]	40	38	39	37	40	37	40	35	40	37.5	39	40
10^{BER}	-1.76	-2.19	-1.65	-1.81	-2.18	-1.93	-1.86	-2.1	-2.14	-2.1	-2.02	-2.7
EVM [dB]	-14.6	-14.3	-13.8	-14.34	-14.08	-12.7	-10.12	-14.26	-14.25	-13.32	-14.79	-15.14

Considering that the tests done with ideal components were not successful in achieving a BER of 10^{-3}, it was expected that the system with the 2nd order super Gaussian filter and SSMF would not perform good as well.

4.4 Conclusions

After presenting the results obtained for each case studied, there are some conclusions that can be made. The first one and the more important is the fact that neither case tested was able to achieve the BER of 10^{-3}, defined in the objectives. This could have been caused by the non-linearity from the electrical to optical modulator used in this work, the DP-MZM; by the incapability of the MP to mitigate the SSBI , by the noise or also caused by simulation errors.

Aside the fact that the objective was not achieved, there was also another value that was not expected, which was the value for the BER of the SB and MB in each case. It was expected that the BER for the SB case, since there is no crosstalk present or harmonics from other bands, would be lower than the MB values, which did not occur. This occurrence could not be explained.

Apart from these results, it was verified that with the introduction of the 2nd order super Gaussian filter instead of the ideal one, the performance of the system was reduced. Also, the effect of the optical fibre was demonstrated to be negligible, due to the fact that the time spread is account for by the CP. Another effect that was verified on the results obtained was the distortion present in each band being different. For example, bands 1 and 12 were supposed to be the bands with better performance results since they are the less affected by crosstalk or harmonics from the other bands. Between these two the 12th band was the one that presented the best values as expected, because during selection the filter would select a small part of the next band. Since this was the last band it caused less distortion in the photodetection process. As expected as well, the bands 6 and 7, being the bands from the middle of the MB-OFDM signal, were the most affected by distortion caused by crosstalk and harmonics of the other bands of the MB-OFDM signal.

Chapter 5 - Final conclusions and future research

5.1 Final conclusions

In this dissertation, the mitigation of the SSBI using MP was evaluated.

In chapter 2, the concept of OFDM was presented in detail. The components of an OFDM system were described and the main advantages and disadvantages of OFDM were depicted. It was concluded that thanks to the orthogonality condition of an OFDM signal, the spectral efficiency achieved could be advantageous. Furthermore, the components of a DDO-OFDM system were singly described, presenting for each the reason behind its usage and their main performance issues. The origin of the SSBI was demonstrated. Continuously, the signal used on this system, the SSB-OFDM signal was presented, jointly with its parameters and the concept of MB-OFDM was depicted. Lastly the parameters of the SSB MB-OFDM signal used on this work were presented. To maintain the high spectral frequency presented at the beginning of chapter 2, a small VBG and SSBI techniques are required. Therefore the MP might me the solution to mitigate the SSBI without compromising the spectral efficiency.

In chapter 3, the MP theory was presented alongside the description of how the MP is used and where it is implemented. With execution of an exhaustive evaluation, it was demonstrated that with a noise free system it was possible to improve the system performance by 7 dB, requiring 87 coefficients. By assessment of the results obtained it was concluded that the number of coefficients used was not proportional to the improvement obtained. However, with the MP structure selected and its coefficients it was possible to understand that the improvement depended on the input symbols of the system. It was not evaluated but it is possible that if it was used an MP with more coefficients, the MP would be able to guarantee the same improvement for a higher number of OFDM symbol sequences. To overcome this limitation issue related to the input OFDM symbol sequences, it was presented and describe a technique that would adapt the coefficients to be able to compensate other OFDM symbol sequences. However, this adaptive approach did not improved the results for other OFDM symbol sequences, which allowed to conclude that its addition to the MB-OFDM system would only require more computer complexity. In this chapter it was also presented the non-ideal filter used on the band selector, the 2nd order super Gaussian model.

In chapter 4, it were presented the results for the assessments executed regarding the performance impact of the non-ideal components such as the 2nd order super Gaussian filter in the band selector and optical fibre in the transmission channel. Each combination of nonlinear component was presented and evaluated. Firstly, with the results for the ideal band selector and B2B configuration it was not possible to achieve the BER of 10^{-3}. Although the system parameters were similar to the system parameters used on chapter 3, it was possible to assess the impact of thermal and optical noise on the system. With the addition of nonlinear components and MB configuration, it would be expected that the BER of 10^{-3} would not be available to achieve. Besides the introduction of noise on the tests executed, it was also introduced more noise, crosstalk and the harmonics of the other bands on the other tests. Therefore it could be concluded that the use of MP would not be able to mitigate the SSBI on the MB-OFDM system evaluated.

5.2 Future research

As it was concluded, the small number of coefficients led to a limitation on the number of OFDM symbol sequences at the input that would be able to achieve an improvement on the SSBI mitigation. As for future work, it would be interesting to evaluate if with MP structures which used 150 or an higher number of coefficients would withstand more OFDM symbol input sequences and therefore mitigate the SSBI distortion.

References

[1] R. Davey, D. Grossman, M. Wiech, D. Payne, D. Nesset, A. Kelly, A. Rafael, S. Appathurai, and S. Yang, "Long-reach passive optical networks," *J. Lightw. Technol.,* vol. 27, no. 3, pp. 273-291, February 2009.

[2] N. Cvijetic, M. Huang, E. Ip, Y. Huang, D. Qian, and T. Wang, "1.2Tb/s symmetric WDM-OFDM-PON over 90km straight SSMF and 1:32 passive split with digitally-selective ONUs and coherent receiver OLT," *Conf. on Optical Fiber Communication,* Los Angeles, CA, USA, March 2011, pp.1-3.

[3] A. Saleh and J. Simmons, "Architectural principles of optical regional and metropolitan access networks," *J. Lightw. Technol.,* vol. 17, no. 12, pp. 2431-2448, December 1999.

[4] W. Wei, D. Xu, D. Qian, P. Ji, T. Wang, and C. Qiao, "Demonstration of an optical OFDMA metro ring network with dynamic sub-carrier allocation," *Conf. on Optical Fiber Communication,* San Diego, CA, USA, March 2009, pp. 1-3

[5] T. Alves, L. Mendes, and A. Cartaxo, "High granularity multiband OFDM virtual carrier-assisted direct-detection metro networks," *J. Lightw. Technol.,* vol. 33, no. 1, pp. 42-54, November 2014.

[6] A. Lowery, L. Du, and J. Armstrong, "Orthogonal frequency division multiplexing for adaptive dispersion compensation in long haul WDM systems," *Conf. on Optical Fiber Communication*, Anaheim, CA, USA, March 2006, pp.1-3.

[7] S. Jansen, I. Morita, and H. Tanaka, "10x121.9-Gb/s PDM-OFDM transmission with 2-b/s/Hz spectral efficiency over 1,000 km of SSMF," *Conf. on Optical Fiber Communication*, San Diego, CA, USA, February 2008.

[8] A. Lowery, L. Du, and J. Armstrong, "Performance of optical OFDM in ultralong-haul WDM lightwave systems," *J. Lightw. Technol.*, vol. 25, no. 1, pp. 131-138, January 2007.

[9] J. Armstrong, "OFDM for optical communications," *J. Lightw. Technol.,* vol. 27, no. 3, pp. 189-204, February 2009.

[10] J. Bingham, "Multicarrier modulation for data transmission: An idea whose time has come," *IEEE Commun. Mag.*, vol. 28, no. 5, pp. 5-14, May 1990.

[11] W. Zou and Y. Wu, "COFDM: An overview," *IEEE Trans. Broadcast.,* vol. 41, no. 1, pp 1-8, March 1995.

[12] R. Dischler and F. Buchali, "Transmission of 1.2 Tb/s continuous waveband PDM-OFDM-FDM signal with spectral efficiency of 3.3 bit/s/Hz over 400 km of SSMF," *Conf. on Optical Fiber Communication,* San Diego, CA, USA, March 2009, pp. 1-3.

[13] T. Pollet, M. Van Bladel, and M. Meneclaey, "BER sensitivity of OFDM systems to carrier frequency offset and Wiener phase noise," *IEEE Trans. Commun.,* vol. 43, no. 2/3/4, pp. 191-193, February/March/April 1995.

[14] E. Le Rouzic, "Network evolution and the impact in core networks," *36th European Conference and Exhibition on Optical Communication,* Torino, Italy, September 2010, pp. 1-8

[15] A. Morea, H. Nakajima, L. Chacon, E. Le Rouzic, B. Decocq, and J. Sebille, "Impact of the reach of WDM systems and traffic volume on the network resources and cost of translucent optical transport networks," *Proc. on Transparent Optical Networks,* vol. 1, pp. 65-68, July 2004.

[16] W. Peng, I. Morita, H. Takahashi, and T. Tsuritani, "Transmission of high speed (>100 Gb/s) direct-detection optical OFDM superchannel," *J. Lightw. Technol.,* vol. 30, no. 12, pp. 2025-2034, April 2012.

[17] Z. Li, X. Xiao, T. Gui, Q. Yang, R. Hu, Z. He, M. Luo, C. Li, X. Zhang, D. Xue, S. You, and S. Yu, "432 – Gb/s direct-detection optical OFDM superchannel transmission over 3040-km SSMF," *IEEE Photonics Technol. Lett.,* vol. 25, no. 15, pp. 1524-1526, July 2013.

[18] M. Shetzen, *The Volterra and Wiener theories of nonlinear systems,* New York: Wiley, 1980.

[19] Y. Shen, B. Hraimel, X. Zhang, G. Cowan, K. Wu, and T. Liu, “A novel analog broadband RF predistortion circuit to linearize electro-absorption modulators in multiband OFDM radio-over-fiber systems,” *IEEE Trans. Microw. Theory Tech.,* vol. 58, no. 11, pp. 3327-3335, September 2010.

[20] A. D’Andrea, V. Lottici, and R. Reggiannini, “Nonlinear predistortion of OFDM signals over frequency-selective fading channels,” *IEEE Trans. Commun.,* vol. 49, no. 5, pp. 837-843, May 2001.

[21] J. Carvers, “Amplifier linearization using a digital predistorter with fast adaptation and low memory requirements,” *IEEE Trans. Veh. Technol.,* vol. 39, no. 4, pp. 374-382, November 1990.

[22] D. Morgan, Z. Ma, J. Kim, M. Zierdt, and J. Pastalan, “A generalized memory polynomial model for digital predistortion of RF power amplifiers,” *IEEE Trans. Signal Process.,* vol. 54, no. 10, pp. 3852-3860, October 2006.

[23] L. Ding, G. Zhou, D. Morgan, M. Zhengxiang, J. Kenney, J. Kim, and C. Giardina, “A robust digital baseband predistorter constructed using memory polynomials,” *IEEE Trans. Commun.*, vol. 52, no. 1, pp. 159–165, January 2004.

[24] Z. Liu, M. Violas, and N. Carvalho, “Digital predistortion for RSOAs as external modulators in radio over fiber systems,” *Optics Express*, vol. 19, no. 18, pp. 17641–17646, August 2011.

[25] Y. Pei, K. Xu, J. Li, A. Zhang, Y. Dai, Y. Ji, and J. Lin, “Complexity-reduced digital predistortion for subcarrier multiplexed radio over fiber systems transmitting sparse multi-band RF signals,” *Optics Express*, vol. 21, no. 3, pp. 3708–3714, February 2013.

[26] Y. Liu, J. Zhou, W. Chen, and B. Zhou, “A robust augmented complexity-reduced generalized memory polynomial for wideband RF power amplifiers,” *IEEE Trans. Ind. Electron.*, vol. 61, no. 5, pp. 2389–2401, June 2013.

[27] T. Alves, J. Morgado, and A. Cartaxo, “Linearity improvement of directly modulated PONs by digital pre-distortion of coexisting OFDM-based signals,” in *Advanced Photonics Congress*, Colorado Springs, CO, USA, June 2012, pp. 1-2.

[28] R. Chang, “Synthesis of band-limited orthogonal signals for multichannel data transmission,” *Bell System Technical J.*, vol. 45, no. 10, pp. 1775-1796, December 1966.

[29] R. Mosier and R. Clabaugh, “Kineplex, a bandwidth-efficient binary transmission system,” *AIEE Trans.,* vol. 76, no. 6, pp. 723-728, January 1958.

[30] M. Zimmerman and Alan L. Kirsch, “The AN/GSC-10 (KATHRYN) variable rate data modem for HF Radio,” *IEEE Trans. Commun. Technol,* vol. 15, no. 2, pp. 197-204, April 1967.

[31] R. Mosier and R. Clabaugh, “Kineplex, a bandwidth efficient binary transmission system,” *Transactions of the American Institute of Electrical Engineers, Part I: Communication and Electronics*, vol. 76, no. 6, pp. 723-728, January 1958.

[32] S. Weinstein and P. Ebert, “Data Transmission by Frequency-Division Multiplexing Using the Discrete Fourier Transform,” *IEEE Trans. Commun. Technol,* vol. 19, no. 5, pp. 628-634, October 1971.

[33] P. Duhamel and H. Hollmann, “Split-radix FFT algorithm,” *IET Electronics Letters*, vol. 20, pp. 14-16, 1984.

[34] S. Hara and R. Prasad, “Multicarrier Techniques for 4G Mobile Communications,” *Boston: Artech House*, 2003.

[35] W. Shieh, and I. Djordjevic, *OFDM for Optical Communications,* Elsevier, USA, 2010.

[36] T. Pollet, M. Van Bladel, and M. Meneclaey, “BER sensitivity of OFDM systems to carrier frequency offset and Wiener phase noise,” *IEEE Trans. Commun.,* vol. 43, no. 2/3/4, pp. 191-193, February/March/April 1995.

[37] L. Tomba, “On the effect of Wiener phase noise in OFDM systems,” *IEEE Trans. Commun.,* vol. 46, no. 5, pp. 580-583, May 1998.

[38] A. Armada, “Understanding the effects of phase noise in orthogonal frequency division multiplexing (OFDM),” *IEEE Trans. Broadcast.,* vol. 47, no. 2, pp.153-159, June 2001.

[39] S. Wu and Y. Bar-Ness, “OFDM systems in the presence of phase noise: consequences and solutions,” *IEEE Trans. Commun.,* vol. 52, no. 11, pp. 1988-1996, November 2004.

[40] K. Sathananthan and C. Tellambura, “Probability of error calculation of OFDM systems with frequency offset,” *IEEE Trans. Commun.,* vol. 49, no. 11, pp. 1884-1888, November 2001.

[41] J. Armstrong, “Analysis of new and existing methods of reducing intercarrier interference due to carrier frequency offset in OFDM,” *IEEE Trans. Commun.,* vol. 47, no. 3, pp. 365-369, March 1999.

[42] Y. Xingwen, W. Shieh, and Y. Ma, “Phase noise effects on high spectral efficiency coherent optical OFDM transmission,” *J. Lightw. Technol.,* vol. 26, no. 10, pp. 1309-1316, May 2008.

[43] D. Fonseca, A. Cartaxo, and P. Monteiro, “Modelling and experimental validation of an x-cut four phase modulators structure,” *IEEE Proceedings Optoelectronics*, vol. 153, no. 4, pp. 145-151, August 2006.

[44] T. Alves and A. Cartaxo, “Performance comparison of power fading mitigation techniques in multiband OFDM-UWB signals transmission along LR-PONs,” *Chin. Opt. Lett.*, vol. 11, no. 8, pp. 080602-1–080602-6, Aug. 2013.

[45] P. Wei-Ren, W. Xiaoxia, V. Arbab, B. Shamee, L. Christen, Y. Jeng-Yuan, F. Kai-Ming, A. Willner, and C. Sien, “Experimental demonstration of a coherently modulated and directly detected optical OFDM system using an RF-tone insertion,” *Conf. on Optical Fiber Communication*, San Diego, CA, USA, February 2008, pp. 1-3.

[46] W. Peng, B. Zhang, F. Kai-Ming, X. Wu, A. Willner. and C. Sien, “Spectrally efficient direct-detected OFDM transmission incorporating a tunable frequency gap and an iterative detection techniques,” *J. Lightw. Technol.,* vol. 27, no. 24, pp. 5723-5735, October 2009.

[47] B. Schmidt, A. Lowery, and J. Armstrong, “Experimental demonstrations of 20 Gbit/s direct-detection optical OFDM and 12 Gbit/s with a colorless transmitter,” *Conf. on Optical Fiber Communication,* San Diego, CA, USA, February 2008.

[48] A. Zhu, P. Draxler, J. Yan, T. Brazil, D. Kimball, and P. Asbeck, “Open-loop digital predistorter for RF power amplifiers using dynamic deviation reduction-based Volterra series,” *IEEE Trans. Microw. Theory Tech.*, vol. 56, no. 7, pp. 1524–1534, June 2008.

[49] H. Cao, H. Nemati, A. Tehrani, T. Eriksson, J. Grahn, and C. Fager, “Linearization of efficiency optimized dynamic load modulation transmitter architectures,” *IEEE Trans. Microw. Theory Tech.*, vol. 58, no. 4, pp. 873–881, March 2010.

[50] F. Carvalho and A. Cartaxo, “Broad baseband nonlinear distortion mitigation using digital pre- and post-distortion in OFDM-based long-reach PON,” *Optics Express*, vol. 23, no. 6, pp. 7062–7074, February 2015.

[51] S. Jansen, I. Morita, and H. Tanaka, “10x121.9-Gb/s PDM-OFDM Transmission with 2-bit/s/Hz Spectral Efficiency over 1,000 km of SSMF,” *Conf. on Optical Fiber Communication*, San Diego, CA, USA, February 2008.

[52] B. Schmidt, A. Lowery, and L. Du, “Low sample rate transmitter for DD optical OFDM,” *Conf. on Optical Fiber Communication*, San Diego, CA, USA, February 2009.

[53] W. Peng, X. Wu, V. Arbab, B. Shamee, L. Christen, J. Yang, K. Feng, A. Willner, and S. Chi, “Experimental demonstration of 340 km SSMF transmission using a virtual single sideband OFDM signal that employs carrier suppressed and iterative detection techniques,” *Conf. on Optical Fiber Communication*, San Diego, CA, USA, February 2008, pp. 1-3.

[54] W. Peng, X. Wu, V. Arbab, B. Shamee, L. Christen, J. Yang, K. Feng, A. Willner, and S. Chi, “Experimental demonstration of a coherently modulated and directly detected optical OFDM system using an RF-tone insertion,” *Conf. on Optical Fiber Communication*, San Diego, CA, USA, February 2008, pp. 1-3.

[55] (2014, May). [Online]. Available: http://www.oclaro.com/product_pages/Scalable_WSS_Family.php.

[56] T. Alves and A. Cartaxo, “Virtual Carrier-Assisted Direct-Detection MB-OFDM Next-Generation Ultra-Dense Metro Networks Limited by Laser Phase Noise,” *J. Lightw. Technol.,* vol. 33, no. 19, pp. 4093-4100, August 2015.

[57] E. Desurvire, “Capacity demand and technology challenges for lightwave systems in the next two decades,” *J. Lightw. Technol.*, vol. 24, no. 12, pp. 4697-4710, December 2006.

[58] G. Agrawal, Fiber-Optic Communication Systems, 3rd edition, Wiley-Interscience, USA, 2002.

[59] ITU-T G.975.1, Forward Error Correction for high bit-rate DWDM Submarine System, February 2004.

[60] ITU-T G.709/Y.1331, Interfaces for the optical transport network, February 2012.

[61] J. Morgado, “Linearization of directly modulated lasers,” Internal Report, Instituto de Telecomunicações, Lisboa, January 2012.

Appendix A - Simulator characteristics

A.1 - DAC

The digital to analogue converter, DAC, is responsible for converting a digital signal into an analogue one. To perfectly represent an analogue signal during simulation, the amount of samples have to be infinite. Since this is impossible to achieve, the number of samples have to finite. As the number of digital samples increase, the representation of the signal is closer to the analogue signal, with the downside of increasing computation time.

The DAC was implemented in two different ways, using ideal sampling and sample & hold. On one hand, the transfer function of the DAC using ideal sampling was given by:

$$H(f) = TF\left\{\text{sinc}\left(2\frac{t}{T_c}\right)\right\} \tag{A.1}$$

where T_c represents the chip time, expressed by:

$$T_c = \frac{T_0}{N}. \tag{A.2}$$

In equation A.2, T_0 represents the information length of the symbol period and N_{sc} the number of subcarriers.

On the other hand, the transfer function of the DAC when the sample & hold was implemented is given by:

$$H(f) = T_s\text{sinc}(fT_s) \tag{A.3}$$

where T_s represents the OFDM symbol period.

A.2 - Thermal noise

Thermal noise is the electrical noise generated by a resistive or active electrical component. This noise is intrinsic to all electrical components and does not depend on the voltage applied to its terminals.

In this dissertation, the noise considered in the system is additive white Gaussian noise (AWGN), generated by the bias resistance of the photodetector. The unilateral power spectral density of the noise generated is given by:

$$S_C(f) = \frac{4k_BTf_n}{R_B}, \tag{A.4}$$

where k_B = 1,38×10^{-23} J/K is the Boltzmann's constant; T is the room temperature, which is frequently considered 290 Kelvin; f_n is the noise factor of the pre-amplifier present in the photodetector and R_B is the bias resistance of the photodetector. In this case, the typical value for $\sqrt{S_C(f)}$ is $1\text{pA}/\sqrt{\text{Hz}}$.

A.3 - Up and down conversion

The up and down conversion is used as a complex to real and real to complex converters, respectively. Since the signal at the transmitter side is in baseband, in order to be up-converted to a RF frequency, the up-converted OFDM signal can be expressed as:

$$x_{OFDM}(t) = x_I(t)\cos(2\pi f_c t + \phi_I) - x_Q(t)\sin(2\pi f_c t + \phi_Q) \tag{A.5}$$

where $x_{OFDM}(t)$ is the output signal of the up-conversion, $x_I(t)$ is the baseband in-phase component and $x_Q(t)$ is the baseband quadrature component, f_c is the up-conversion frequency, ϕ_I is the phase of the cosine of the up-converter and ϕ_Q is the phase of the sine of the up-converter.

At the receiver side, the down-conversion is executed backwardly. Therefore, the output signals of the down-conversion can be expressed by:

$$\begin{aligned} y_I(t) &= y_{OFDM}(t)\cos(2\pi f_{dc} t + \phi_{I,dc}) \\ y_Q(t) &= -y_{OFDM}(t)\sin(2\pi f_{dc} t + \phi_{Q,dc}) \end{aligned} \tag{A.6}$$

where $y_I(t)$ and $y_Q(t)$ are the in-phase and quadrature components of the OFDM signal after the down-conversion, $y_{OFDM}(t)$ is the received OFDM signal at the input of the down-converter, f_{dc} is the down-conversion frequency, $\phi_{I,dc}$ is the phase of the cosine of the down-converter and $\phi_{Q,dc}$ the phase of the sine of the down-converter.

However, the phases of the cosine and the sine in the up-conversion, which are considered zero, are different from the phases of the cosine and sine of the down-conversion. This occurs because of the channel not being ideal. But, in order to perform the down-conversion correctly, during simulation, an auxiliary signal is transmitted alongside the MB-OFDM signal. This auxiliary signal is composed by the central frequency of the OFDM bands and its corresponding virtual carrier frequencies. After the auxiliary signal is processed in the PIN, its output contains the sinusoidal wave with the adequate phase to perform the down-conversion.

Also, since this is a MB-OFDM system, where virtual carriers are used, the down-conversion frequency is different from the up-conversion frequency. In this case the down-conversion frequency is f_c-f_{vc}, where f_{vc} is the frequency of the virtual carrier.

A.4 - Equalizer

The communication channel used during the transmission of the OFDM signal is affected by dispersion. In order to overcome this effect, an equalizer is needed. An equalizer is used to estimate the distortion induced by the channel. This estimation is done by using training symbols to evaluate the channel transfer function, which is the inverse of the equalizer transfer function. The channel transfer function is given by:

$$T_{n,k} = \frac{Y_{n,k}}{X_{n,k}} \tag{A.7}$$

where *Y* represent the received QAM training symbols, *X* the transmitted QAM training symbols, *n* the OFDM symbol and *k* the subcarrier. This transfer function is evaluated for each subcarrier. Then the mean value is calculated in order to eliminate the noise effect (because the AWGN medium is zero). At the end, when the channel transfer function is estimated and consequently the equalizer transfer function, it is applied to the OFDM information symbols to compensate the distortion of the channel.

A.5 - EVM

In this dissertation, one way of evaluating the performance of the system developed is using the error vector magnitude (EVM). When a signal is sent through an ideal system, the transmitted symbols are equal in amplitude and phase to the received symbols. But, in a real system, where noise and distortion exist, the transmitted symbols are different from the received ones. The EVM is then used to evaluate the quality of a digital transmission. In order to perform such evaluation, the EVM is achieved by calculating the difference of amplitude and phase between the received symbols and the ideal symbols. In figure 2.23, it is represented an illustration of how the EVM is calculated, in which the blue cross represents the location of the ideal symbol and the red cross the location of the received signal. The EVM value is then given by the error vector length between these two symbols.

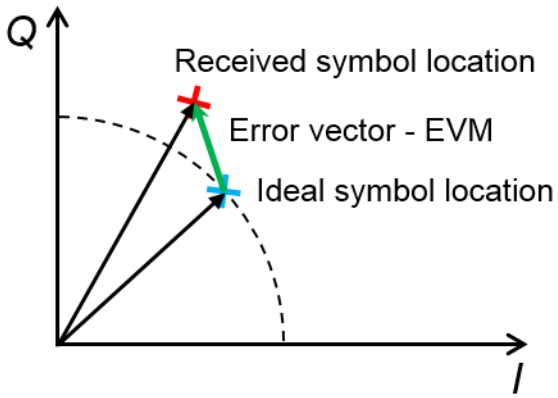

Figure A. 1 - Illustration of the error vector magnitude (EVM).

The EVM of an OFDM signal is defined, per *k*-th subcarrier, by the mean-square value of the error magnitude between received symbols and ideal symbols and it is given by:

$$EVM[k] = \frac{\left\langle \left| s_o^{(l)}[k] - s_i^{(l)}[k] \right|^2 \right\rangle}{\left\langle \left| s_i^{(l)}[k] \right|^2 \right\rangle} \quad , \quad EVM = \left\langle EVM[k] \right\rangle \tag{A.8}$$

where *k* represents the subcarrier, $s_o^{(l)}[k]$ the QAM symbol of the *k*-th subcarrier and *l*-th OFDM symbol obtained at the equalizer output and $s_i^{(l)}[k]$ the ideal QAM symbol of the *k*-th subcarrier and the *l*-th OFDM symbol.

With the EVM it is possible to evaluate the BER. This can be done through expression A.9. This expression gives the BER for each subcarrier of the signal.

$$BER[k] = 2\frac{1-\frac{1}{\sqrt{M}}}{M-1} erfc\left[\sqrt{\frac{3\log_2\sqrt{M}}{M-1}\frac{1}{EVM_{RMS}^2[k]\log_2 M}}\right]$$
$$BER = \frac{1}{N_{sc}}\sum_{k=1}^{N_{sc}} BER[k] \quad \text{(A.9)}$$

A.6 - Optical noise

Optical noise is the noise generated on the optical amplifier, which is used to compensate the fibre losses. Since the system designed on this work operates on the C-band, the optical amplifier chosen is the erbium-doped fibre amplifier. The noise added to the system is originated during the process of signal amplification, in which the EDFA amplifies the spontaneous emission generated in its interior. The spectral density of the amplified spontaneous emission (ASE), S_{ase}, is given by

$$S_{ASE} = h\nu_0 f_n (g-1) \quad \text{(A.10)}$$

Where h is the Planck's constant, ν_0 the optical frequency, f_n the noise factor (7 dB in this work) of the EDFA and g the optical amplifier gain.

The ASE noise affects the signal in four different components. These components derive from the polarizations of the optical fibre and the two components of the MB-OFDM signal. On one hand, the optical fibre has two different polarizations orthogonal to each other, the parallel (||) and the perpendicular (⊥) polarization. On the other hand, the MB-OFDM is composed by the in-phase (I) and quadrature (Q) components. Similar to the signal, the noise also has an in-phase and a quadrature components, which means that for each optical fibre polarization, there is a pair of in-phase and quadrature components. Therefore, the spectral density of the ASE noise is divided by each component, represented in expression A.11

$$S_{ASE,||,I} = S_{ASE,||,Q} = S_{ASE,\perp,I} = S_{ASE,\perp,Q} = \frac{S_{ASE}}{4} \quad \text{(A.11)}$$

Considering that the electrical field propagates in the || polarization, and that the ASE noise propagates on both || and ⊥ polarizations, the output of the EDFA can be expressed in expression A.12

$$e_{EDFA,out}(t) = \left[e_{EDFA,in,I}(t) + je_{EDFA,in,Q}(t) + n_{ASE,||,I} + n_{ASE,||,Q}\right]_{e_{||}} + \left[n_{ASE,\perp,I} + n_{ASE,\perp,Q}\right]_{e_\perp} \quad \text{(A.12)}$$

Where $e_{EDFA,in}$ is the in-phase optical field component of the OFDM signal at the EDFA input, $n_{ASE,||,I}$ and $n_{ASE,||,Q}$ are the parallel ASE noise components and the others are the perpendicular components of the ASE noise.

Finally, considering the expression 2.28, PIN output current can be given by

$$i_{PIN}(t) \propto \left|e_{EDFA,out}(t)\right|^2 = \left|e_{EDFA,in}(t) + e_{n,||}(t)\right|^2 + \left|e_{n,\perp}(t)\right|^2 \quad \text{(A.13)}$$

where $e_{n,||}(t)$ and $e_{n,\perp}(t)$ are the noise optical field for the parallel and perpendicular polarization.